Mahdi Pahlevan

Silk-inspired molecular design of bacterial nanocellulose biomaterials

Åbo Akademi University

Mahdi Pahlevan

Born 1984

Previous studies and degrees

Master, Åbo Akademi University, 2011

Bachelor, Sharif University of Technology, 2008

Silk-inspired molecular design of bacterial nanocellulose biomaterials

Mahdi Pahlevan

Laboratory of Natural Materials Technology
Faculty of Science and Engineering
Åbo Akademi University
Åbo, Finland, 2020

Supervisors
Adjunct Professor Parvez Alam
School of Engineering
Institute for Materials and Processes
University of Edinburgh
EH8 9YL, Edinburgh, UK

Professor Martti Toivakka
Laboratory of Natural Materials Technology
Faculty of Science and Engineering
Åbo Akademi University
FI-20500 Turku, Finland

Examiners
Professor Mikael Skrifvars
Department of Resource Recovery and Building Technology
University of Borås
SE-503 32 Borås, Sweden

Associate Professor Henrikki Liimatainen
Laboratory of Fibre and Particle Engineering
Faculty of Technology
Oulu University
FI-90014 Oulu, Finland

ISBN 978-952-12-3971-7
ISBN 978-952-12-3972-4 (pdf)
Painosalama Oy – Turku, Finland 2020

To my wife

Preface and Acknowledgements

This work was carried out at the Laboratory of Paper Coating and Converting (Paf), from January 2012 to December 2017. There were no industrial partners involved in this project. However, there were collaborations with other laboratories for acquiring materials, equipment, etc. The financial support for this project was from various foundations. Sincere appreciation for financial support from the Åbo Akademi foundation, the Ella and George Enhrooth Foundation, the Otto Malm Foundation, Harry Elvings Foundation and the Rector of Åbo Akademi University.

I am immensely grateful to my supervisor Adjunct Prof. Parvez Alam for providing me with the wonderful opportunity to carry out this doctoral work and learn a great deal about material world from him. Your passion for discovery, enthusiastic view to biomimetic science and encouragement were my main source of inspiration throughout my doctoral studies. I really appreciate the time and trust you put in this work and your support not just as a supervisor but as an older brother in the difficult times I had. I sincerely appreciate Prof. Martti Toivakka as my co-supervisor for his kind guidance and support scientifically and financially throughout my studies and I am grateful for your valuable talks and advices to improve my abilities as a researcher.

I had been also honoured to be part of Paf family in Turku. I would like to thank all the Pafers for their kindness and support in my time in Finland. I want to specially thanks Mari Nurmi, for her kindness and willingness to help for many issues one can face at work and helping me with translation of abstract into Swedish. Sincere thanks to ÄV, Jani, Pauliina, and Peter for ensuring that all the equipment in the laboratory worked without hiccups. I am really grateful of my officemate and good friend Diosa, for her friendship and great discussions we had. I sincerely appreciate the company of Farid, Vinay, Rajesh, Roger, Anni, Milena, Kofi, Mukunda during my time at Paf and outside work. Special thanks to Joel whom I know from the first day I arrived in Finland. We started as Master student and shared lots of good memories and grew old together. Thanks for your support and friendship throughout this 7 years.

Being away from homeland, you need to find your second family. I specially want to thank my best friend Hamid. Meeting you and having you as a friend was the best thing that could happen for me. I couldn't imagine how I could live a better life without your kindness and guidance. Big thanks to my Iranian friends in Finland who

took care of me during the best and worst times, specially Pouya, Fahimeh, Masoud, Azin, Kambiz, Maryam, Mo, Masoumeh and many others. I appreciate your impeccable kindness and friendship.

Finally, last but by no means least, I am deeply grateful of my family, my parents and my sisters. To my dad who is the strongest pillar in my life, my mom who without her kindness and care, my life was meaningless and my sisters, Sara, Maryam and Mohadeseh who are the best siblings in the world. Also I would like to mention my extended family, my parents in law and my siblings in law who are always supportive and caring. I am forever grateful of you.

To my love, Maryam, words cannot describe how much I love you. You stayed by me during the most troubling times in my life and nourished me with your priceless love and affection. You are the true source of happiness, thanks for who you are and for everything you've done for me.

Mahdi Pahlevan

April 2018

Revised in June 2020

Abstract

In recent years, there has been a growing interest in the development of bio-inspired materials as they have the potential to offer improvements in the design of superior mechanical performance materials. Furthermore, the progress of analytical and synthetic methods, provides a more thorough understanding of the molecular and structural mechanisms of bio-materials. Spider silk is an interesting example of a material with extraordinary mechanical behaviour, exhibiting both high tensile strength and considerable elasticity, which results in an exceptional toughness that is superior to most natural or man-made fibres.

The application of spider silk goes way back in history where man-kind used cobwebs as sutures for bleeding wounds or orb webs for fishing. Traditionally, the main factor of inspiration for man-kind was the construction and design of web, however, nowadays research into the material structure and properties of spider silk has opened up new opportunities for spider silk inspired materials in fields as diverse as medical and military. These are sectors that can benefit from high mechanical stability and biocompatibility, which spider silks provide.

The cannibalistic nature of spiders has limited the production of natural spider silk via farming techniques. This has intensified the investigation of various types of silk protein molecular building blocks, their self-assembly properties and the fibre spinning process. Here, we focused on the first two and later modelled this molecular structure in a composite material to gain a better understanding of its mechanical behaviour.

Keywords;

Material science, Spider silk, Dragline silk, Flagelliform silk, Mechanical properties, Molecular dynamics simulation, Bacterial cellulose, Amino acid, bioglue, TEMPO-oxidation

Svensk Sammanfattning

Under de senaste åren har intresset för utveckling av naturinspirerade material ökat eftersom dessa material kan erbjuda förbättringar i materialdesign av mekaniskt utomordentligt starka material. Utveckling av analytiska och syntetiska metoder erbjuder en bättre förståelse av naturmaterialens molekylära och strukturella mekanismer. Spindelsilke är ett intressant exempel av material med märkvärdigt mekaniskt beteende som har både hög dragstyrka och betydande elasticitet, vilket resulterar i en ovanlig seghet som är överlägsen jämfört med största delen av naturliga eller syntetiska fibrer.

Användning av spindelsilke går långt tillbaka i historien då människor använde spindelsilke som suturtråd för blödande sår eller hjulspindelnät för fiske. Traditionellt har nätets konstruktion och design varit huvudorsakerna till intresset men numera har forskningen av materialstruktur och -egenskaper av spindelsilke öppnat nya möjligheter för spindelsilkesinspirerade material t.ex. i medicinska och militära applikationer. Dessa områden kan utnyttja den höga mekaniska stabiliteten och biokompatibiliteten som spindelsilke har.

Den kannibaliska naturen av spindlarna har begränsat produktionen av naturligt spindelsilke genom farmning. Detta har intensifierat undersökningen av olika typer av byggstenar i silkesprotein, deras självmonteringsegenskaper och fiberspinningsprocessen. I detta arbete fokuserades på de två första och senare modellerades denna molekylära struktur till ett kompositmaterial för att bättre kunna förstå dess mekaniska beteende.

Nyckelord;

Materiallära, spindelsilke, storampullsilke, flagellumliknande silke, mekaniska egenskaper, simulering av molekylär dynamik, bakteriell cellulosa, aminosyra, biolim, TEMPO-oxidering

List of original publications

Publication I Pahlevan, M.; Toivakka, M.; Alam, P. Electrostatic charges instigate 'concertina-like' mechanisms of molecular toughening in MaSp1 (spider silk) proteins. **Materials Science and Engineering C**, v. 41, p. 329-334, 2014.

Publication II Pahlevan, M.; Alam, P. Flagelliform silk inspired free amino acid bio-glues in bacterial cellulose biomaterials. **Polymer**, v. 97, p. 122-130, 2016.

Publication III Pahlevan, M.; Toivakka, M.; Alam, P. Mechanical properties of TEMPO-oxidised bacterial cellulose-amino acid biomaterials. **European Polymer Journal**, 2018.

Publication IV Morin, A.; Pahlevan, M.; Alam, P. Chapter 8: Silk Biocomposites: Structure and Chemistry. In: THAKUR, V. **Handbook of Composites from Renewable Materials**. [S.l.]: John Wiley and Sons, 2017. p. 189-205.

Author's contribution

Publication I: Electrostatic charges instigate 'concertina-like' mechanisms of molecular toughening in MaSp1 (spider silk) proteins.

The author planned the work together with Parvez Alam, the author was responsible for performing molecular dynamics simulations. Furthermore, the author analysed the results and wrote the manuscript.

Publication II: Flagelliform silk inspired free amino acid bio-glues in bacterial cellulose biomaterials.

The author planned the work together with Parvez Alam. The author prepared the experimental setup for composite sample manufacture and chemical and mechanical tests. The author also performs molecular dynamics simulations, analysed the results and wrote the manuscript.

Publication III: Mechanical properties of TEMPO-oxidised bacterial cellulose-amino acid biomaterials.

The author planned the work together with Parvez Alam. The author prepared bacterial cellulose and synthesised the TEMPO-oxidised BC. The author also manufactured test samples along with chemical and mechanical tests. Furthermore, the author performed and analysed molecular dynamics simulation and wrote the manuscript.

Publication IV: Silk Biocomposites: Structure and Chemistry

The author wrote part of manuscript regarding molecular structure and material properties of spider silk protein.

Table of Content

1. Introduction

Composite materials (materials made of two or several components which has different characteristics from the individual components) have been used widely to produce unique materials with improved mechanical performance, chemical activity and various functionalities. Industry takes advantage of composite materials to produce lightweight, durable, non-corrosive, non-conductive, flexible, low maintenance materials. Composites offer several advantages over conventional engineering materials like wood and metals.

Biomaterials and natural fibres are good candidates for the production of nature-friendly composite materials that can be used in various medical and non-medical applications. These materials are mostly non-toxic and do not cause any inflammatory response when contacting human tissues. The most abundant biomaterial in the nature is cellulose. Cellulose can be extracted from different sources e.g. wood and bacterial secretion, and is the structural component of plant and algal cell walls. Though stiff and strong, cellulose has a low toughness, that might be adjustable by using additive materials to create a tougher composite.

Spider silks are amongst the toughest materials in the nature, with the ability to withstand the loading impact of prey flying at speeds exceeding 3 ms^{-1} towards the net (Ortega-Jimenez & Dudley, 2013). Dragline silk has strength on par with synthetic fibres like Kevlar, and flagelliform silk protein can stretch up to three times its original length (Hayashi & Lewis, 1998; Florence Teulé et al., 2012). The outstanding properties of spider silk has made this material interesting for various industrial and biomedical applications.

In this thesis, I try to understand the chemical and mechanical structure of spider silk proteins and study the secondary structure of proteins as the main factor in the determination of a silk's mechanical performance. Initially, I studied the effect of electrostatic charges on the intermolecular interactions and tensile strength of dragline silk using molecular dynamics methods. I hypothesised that electrostatic charges instigate 'concertina-like' mechanisms of deformation of MaSp1 (major ampullate spidroin 1) protein, which would toughen up the dragline silk threads prior to insect-web contact. Furthermore, the adhesive mechanism of flagelliform silk to cellulose was studied. Here, MD simulations reveal that the separate amino acids

(alanine and glycine) can perform on par with flagelliform silk in BC (bacterial cellulose) composite and experimental evidence confirmed a considerable percentage increase in tensile strength of BC composite. I also studied the mechanical properties of amino acid modified TEMPO oxidised BC as it offers an additional functionalisation on the surface of BC, however, it resulted in an inferior mechanical strength as compared to BC composite with free amino acids. The chart below illustrates the roadmap leading to this thesis.

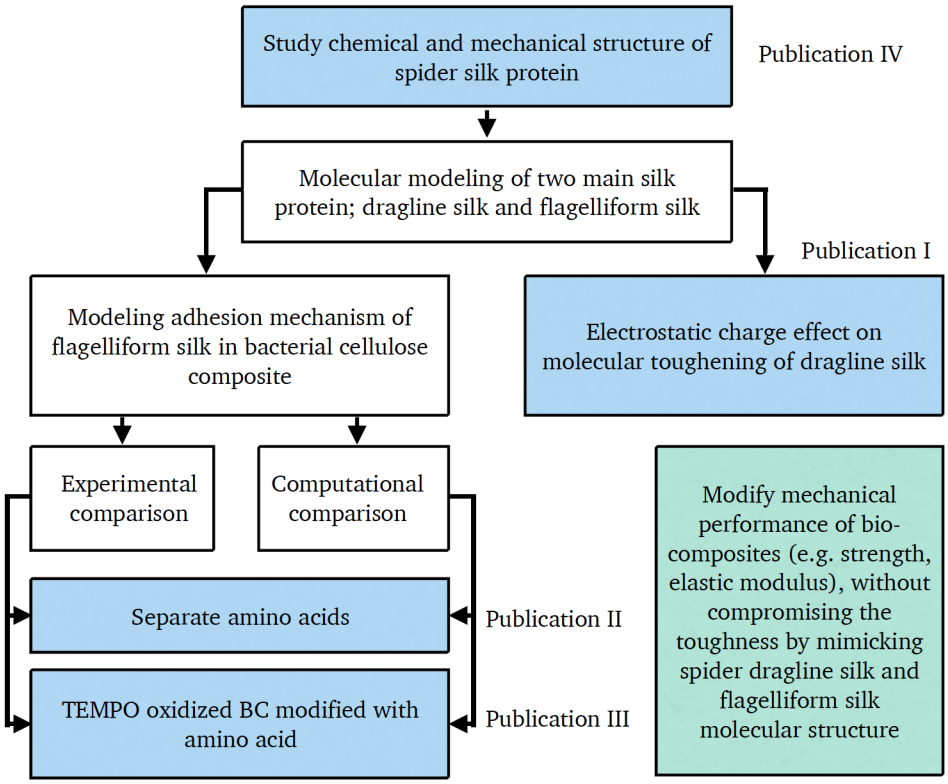

Figure 1 – Flow diagram indication the progression of the thesis

Table 1 - List of abbreviations

AA	Amino Acid
Ala	Alanine
BC	Bacterial cellulose
BC-AA	Bacterial cellulose-based composite with monomeric amino acid
E. coli	Escherichia coli
EDAC	N-ethyl-N-(3-dimethylaminopropyl)-carbodiimide hydrochloride
Flag	Flagelliform Silk
Gly	Glycine
MaSp	Major ampullate
MiSp	Minor ampullate
NHS	N-hydroxy-succinimide
Pro	Proline
TEMPO	2,2,6,6-tetramethylpiperidine-1-oxyl
TOBC	TEMPO oxidised bacterial cellulose
TOBC-AA	Amino acid modified TEMPO oxidised bacterial cellulose

2. Background

Spider silk proteins have been a huge topic of interest in material science due to their outstanding properties of toughness. There are around 40,000 known species of spiders, each producing various types of silk protein in which half of them are used for catching prey (Römer & Scheibel, 2008). Each type of silk protein is produced from wide range of glands, ducts and spigots which have evolved over millions of years for specific application, resulting in function specific mechanical properties. The orb weaving spider (*Nephila Clavipes*), for instance, is one of the most studied spider species, and can produce up to 7 types of silk proteins.

The spinning process of spider silk starts with highly concentrated, unfolded protein dope which is secreted and stored in the spinning glands. The process is highly dependent on the surrounding environmental conditions (Chen, Shao, & Vollrath, n.d.) and requires accurate control over environmental elements such as pH, ionic concentration, and the water content in the spinning glands and ducts. The protein dope (up to 50 % w/v) is stored in primarily a random coil structure within the gland and assembles while passing through the spinning duct (Hijirida et al., 1996). Initially the dope passes through an ion exchange channel wherein phase separation takes place. The process involves ion exchange between chaotropic sodium and chloride ions by kosmotropic potassium and phosphate, and water extraction during passage along the duct (Rising, Widhe, Johansson, & Hedhammar, 2011). There are two theories addressing the mechanism of silk fibre assembly. One proposes the spinning dope has a liquid crystalline behaviour and it can be considered as the reason for the formation of intermolecular interactions such as van der Waals and hydrogen bonds between neighbouring molecules (Keten & Buehler, 2010a). Following this stage, by losing the solvent the protein dope will find its assembled configuration at steady state and will be drawn out of the spinning duct. The alignment of proteins in solution increases by an increase in the flow rate; therefore, stiffer, stronger, but less extensible fibres are achieved through the formation of aligned β-sheet crystalline regions (Chen et al., n.d.; J. G. Hardy, Römer, & Scheibel, 2008). The second theory is based on micellar organisation of the protein prior to elongation to form the thread assembly. Mechanical factors such as reeling speed and shear stresses in the drawing of the silk thread can further adjust the amorphous and crystalline segmentation of silk.

Table 2 - Mechanical properties of natural and synthetic fibres **(Teulé F. , et al., 2012) (Römer & Scheibel, 2008)**

Material	Density [$g.cm^{-3}$]	Strength [GPa]	Elasticity [%]	Toughness [$MJ.m^{-3}$]
MaSp silk	1.3	~4	27	180
Flag silk	1.3	~1	270	150
Insect silk	1.3	0.6	18	70
Nylon 6.6	1.1	0.95	18	80
Kevlar 49	1.4	3.6	2.7	50
Carbon fibre	1.8	4	1.3	25
Steel	7.8	1.5	0.8	6
Rubber	1.1	0.001	600	0.08
Bacterial Cellulose	1.25	~0.2-0.4	~1-5	~40-90

There are other types of silk proteins including; piriform silk which is used primarily in web scaffolding connection joints and the attachment of the net frame to the surrounding materials, and the minor ampullate glands which produce temporary frames to stabilize and support dragline silk, providing thus a template for flagelliform silk fibres. Types of silk glands in the European garden spider *Araneus diadematus* are depicted in Figure 2.

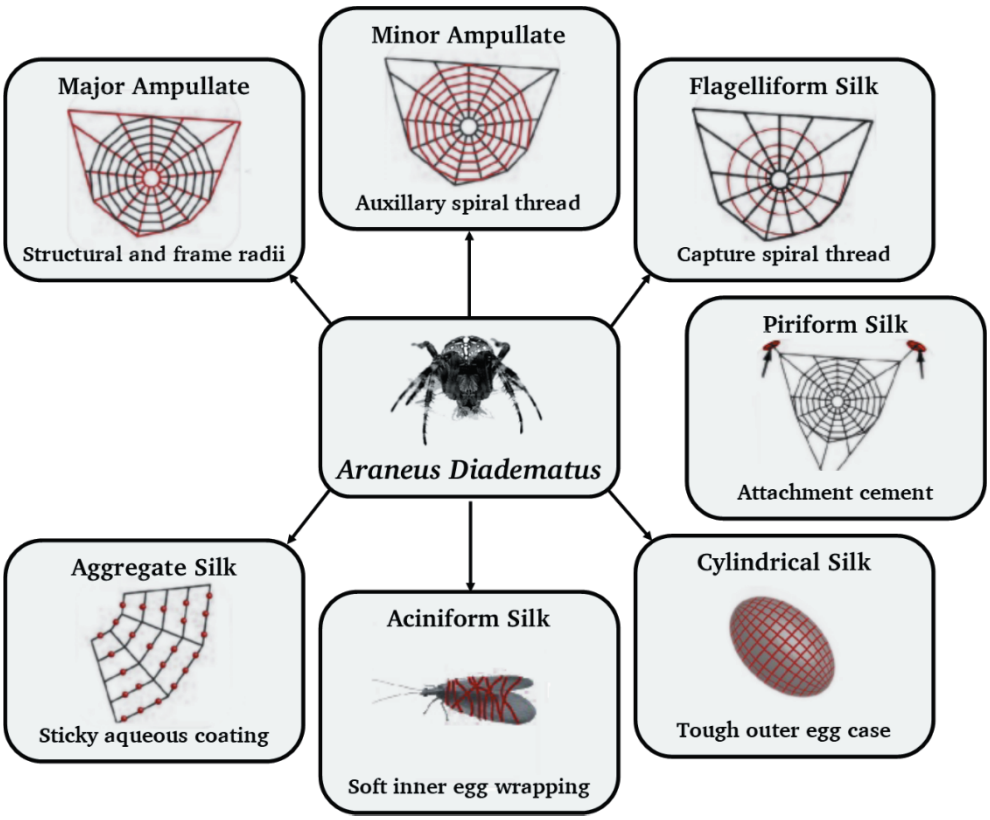

Figure 2 – Schematic overview of different types of spider silk as produced by female orb weaving spiders such as the European garden spider *Araneus diadematus* (adapted from **(Eisoldt, Smith, & Scheibel, 2011)**)

Spider silk protein is mainly rich in nonpolar and hydrophobic amino acids like glycine and alanine, and displays a modular structure consisting of a long repeating protein sequence within the large core domain that is flanked by non-repetitive conserved N- and C-terminal regions. Repeating units in the protein sequence can be further subdivided in shorter amino acid motifs and non-repetitive (NR) regions are in the amino- and carboxyl termini of the proteins. Amino acid motifs are formed by large-scale hydrogen bonding between protein strands and create secondary structures of protein strand, which can be categorized by four distinct motifs; highly crystalline alanine rich β-sheet stacks of A_n or $G(A_n)$, GPGXX motifs that form elastic β-turn spirals, GGX, and spacers (An, Hinman, Holland, Yarger, & Lewis, 2011; Cranford & Buehler, 2012; Keten & Buehler, 2010a; Spiess, Lammel, & Scheibel, 2010).

The motifs account for functionality of silk proteins; for instance, dragline silk contains GGX and GA_n motifs. The GGX (X is typically of alanine, tyrosine, leucine or glutamine) motif is the main group giving dragline silk a moderate elasticity, forming amorphous 3_1 helical structures. Contrarily, alanine rich GA_n or A_n domains form β-sheet stacks that are highly crystalline and contribute to the strength to the silk strands.

Table 3 - Amino acid composition (%-wt) in different types of silk (adapted from **(Lombardi & Kaplan, 1990)**)

Amino acid	*Bombyx Mori*	*Nephila clavipes* (Dragline reeled)	*Nephila Clavipes* (glandular)	*Argiope auranti* (dragline reeled)	*Neoscona domhiliorum* (dragline reeled)
Gly	44.1	37.1	38.1	34.7	38.0
Ala	29.7	21.2	23.4	22.2	18.0
Ser	12.4	4.5	3.9	5.1	6.8
Tyr. Phe	7.5	10.2	4.3	3.8	3.7
Leu. Ile. Val	3.6	11.7	16.6	19.2	2.4
Asx. Glx					
Thr	1.2	1.7	2.0	0.8	0.9
Arg	1.5	7.6	7.2	2.9	0.6
Trp	0.5				
Pro		4.5	3.9	6.4	11.2
His. Cys. Lys		1.0	1.9	0.8	0.9

2.1. Spider silk protein

Spidroins (Sp) of the major (Ma) and minor (Mi) ampullate glands are MaSp1 and MaSp2 (Major) and MiSp1 and MiSp2 (Minor). These spidroins have high molecular weights (200–350 kDa or larger) (Teulé F. , et al., 2012) and are special as they are composed of predominantly alanine and glycine. Amino acid compositions are provided for a variety of silks in Table 3. The MiSp1 and MiSp2 have a higher percentage of polyalanine units than the MaSp1 and MaSp2, which provide greater structural stability and extra support for temporary scaffolds. The polyalanine or

polyglycine–alanine sequences form highly stable β–sheets because of protein folding and amino acid orientation during fibre extrusion. During spinning, liquid–crystal dope from the ampullate major gland is drawn through a tapered duct (Chen, Shao, & Vollrath, 2006) (Vollrath & Knight, 2001). The silk proteins resultantly elongate and align giving rise to hydrogen bonding that form readily due to the polypeptide structures (Vollrath & Knight, 2001). Though hydrogen bonds are weak (5–20 kcal/mol), when there are many forming an interconnected network, the structure becomes significantly more stable. In fact, β–sheet nanocrystals have the dual characteristics of stiffness and flexibility thanks to these H–bond arrays (Keten & Buehler, 2010a). The amorphous regions of dragline silk are rich in glycine arranged into 3_1 helices with type II β–turns (Sintya & Alam, 2016b). By varying the spinning speed, the spider is thus able to control the final structural character of the silk according to requirement (Sintya & Alam, 2016b; Fritz Vollrath, 2000). Fibres spun at higher speeds tend to be highly crystalline as a result of greater protein alignment and thus the formation of higher levels of crystalline β–sheets. When a spider requires greater extensibility and energy dissipation, such as in a frame thread, it spins the fibres more slowly, which increases the ratio of amorphous polymer to crystalline polymer. Dragline silk at the macro level has a five–layer assembly (Sponner, et al., 2007) consisting of the lipid layer, the glycol layer, the skin layer, the outer layer and the inner layer, Figure 3. The main structural components of silk (MiSp and MaSp) are within the core layers. The semi–amorphous domains are rich in glycine, and polyalanine segments within these domains are normally less ordered than in the polyalanine richer domains (Simmons, Michal, & Jelinski, 1996). The crystalline region of MaSp1 is rich in alanine and has both parallel and anti-parallel conformations. Parallel β-sheets have higher stability due to the zig-zag patterned hydrogen bond network, which provides flexibility and connectivity. The orientation of hydrogen bonds along the axis of molecules in antiparallel conformation, provides stable β-sheet nanocrystals. Therefore, this results in stiffer structure compare to parallel conformation, even though it is less flexible and perhaps more brittle in nature (Sintya & Alam, 2016b, 2016a).

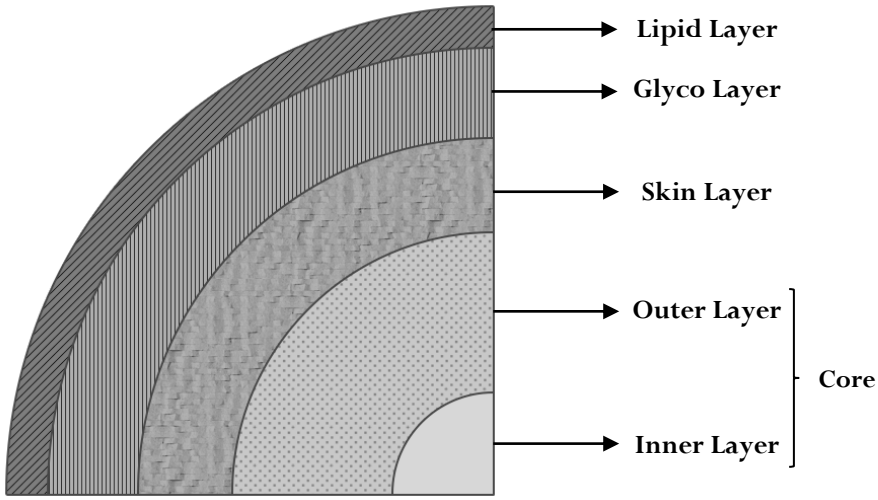

Figure 3 - Layered structure of dragline silk (adapted from (Alexander Morin, Pahlevan, & Alam, 2016))

2.1.1. Dragline silk

Dragline silk is the strongest and toughest type of silk which is used for the frame and radius of the net. Spiders also drag this type of silk as a lifeline when escaping from a predator. Dragline silk is produced from the major ampullate gland. The dragline silks tensile strength can exceed 4 GPa (Teulé F. , et al., 2012) which is comparable to man-made fibres such as Nylon and Kevlar and it can extend up to 30% of its original length when subjected to load. Flagelliform silk is used to construct the capture spiral threads which are produced in the flagelliform gland, and it is weaker than dragline silk (1 GPa) (Teulé F. , et al., 2012). These fibres are extremely elastic and can stretch up to 3 times their original length, making it suitable for capturing prey. When the prey crashes into the net with a very high kinetic energy, the flagelliform silk fibres are able to dissipate the impact energy of the prey (J. Hardy, Science, & 2010, n.d.).

Dragline silk consists of β-sheet crystals that have crosslinking domains forming a network of hydrogen bonds, embedded in a semi-amorphous glycine rich matrix. The crystalline segments have dimensions of a few nanometres and constitute at least 10–15% of the silk volume (Fu, Shao, & Fritz, 2009a; J. G. Hardy et al., 2008; Römer & Scheibel, 2008). Furthermore, the zipped structure of a β-sheet increases the strength

and improves the self-healing properties (Bratzel & Buehler, 2012a). The minimum number of alanine groups to create a β-sheet is 3 alanine groups, but a stable β-sheet requires 6 alanine groups, however, there is no mechanical improvement beyond 8 monomer units (Mahdi Pahlevan, Toivakka, & Alam, 2014; Römer & Scheibel, 2008).

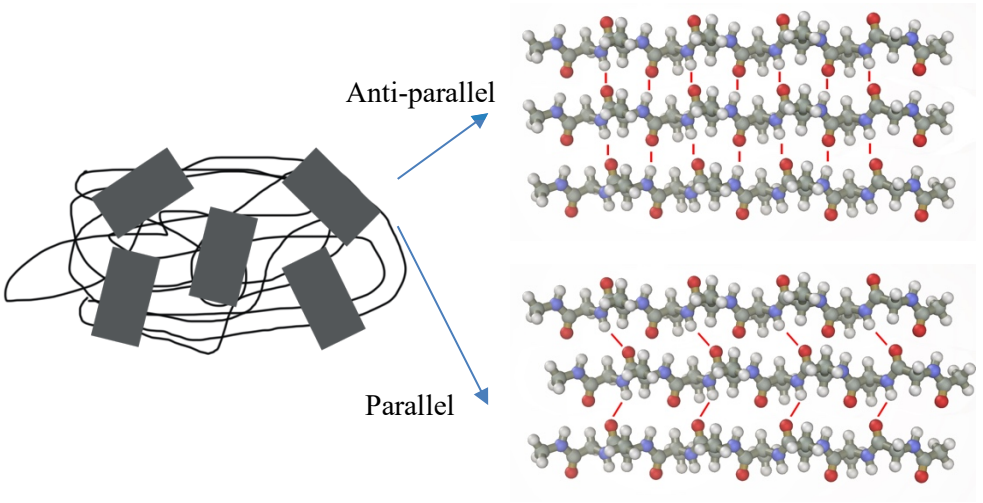

Figure 4 – β-sheet nanocrystal is immersed in a semi-amorphous protein, and parallel and antiparallel orientations of alanine in β-sheets, Antiparallel β-sheet is significantly more stable due to the well aligned H-bonds.

Dragline silk protein contains GGX motifs wherein X typically stands for alanine, tyrosine, leucine or glutamine. These motifs create amorphous 3_1 helical segments of protein that can elongate significantly to dissipate imposed forces. Moreover, alanine rich A_n and GA_n domains form β-sheet nanocrystals which are responsible for the high strength of the protein strand. Antiparallel β-sheet crystals have crosslinking domains which create a network of hydrogen bonds, embedded in a semi-amorphous glycine rich matrix. There are various factors affecting the final secondary structure of spider silk protein such as chemical and mechanical interactions (Grunwald, Rischka, Kast, Scheibel, & Bargel, 2009). The alanine rich and glycine rich motifs form α-helical, β-turns and random coil conformations, respectively (Hakimi, Knight, Vollrath, B, & 2007, n.d.; Scheibel, 2004).

2.1.2. Flagelliform silk

The capture spiral has only half the tensile strength of major ampullate silk, though it has an impressive extensibility of up to 3 times of its original length. The combination of strength and stretchiness give the capture spiral a toughness greater than that of bone, elastin, tendon, silkworm silk, high-tensile steel, Kevlar, and synthetic rubber. In addition to flagelliform protein, the non-fibrous, sticky aggregate silk is the other integral component of the capture spiral. The presence of this glue increases the extensibility of flagelliform silk by providing an aqueous coating. In the capture thread, however, flagelliform silk fibres are what actually stretch then recoil when an insect hits the web (Hayashi & Lewis, 1998).

The high elasticity of flagelliform silk originates from the secondary structure of the silk protein. According to data from Raman spectroscopy data, flagelliform dope is in a highly disordered state within the flagelliform gland and furthermore, compared to dragline silk, flagelliform silk does not show any structural reorganisation and alignment through the spinning process (Teulé F. , et al., 2012). During the self-assembly process of Flag, repeating units form a combination of specific structural amino acid motifs which create the secondary structure of flagelliform silk. The main repeating structural feature of flagelliform silk is GPGGX – where X can be Ala, Val, Ser, or Tyr, which forms type II β-turns and the resulting series of consecutive –up to 63 times before interruption by GGX- β-turns are thought to form a β-spiral (Hayashi & Lewis, 1998). GGX form 3_{10} helices which are also present in dragline silk. The GGX motif is attached to a spacer. There is no definite explanation for the role of a spacer in the protein; however, its presence of mostly negatively charged amino acid (Asp, Glu) suggests an important role nonetheless. This modular structure creates a spring-like structure in its secondary structure, which accounts for the high elasticity of flagelliform silk.

The prey-capturing adhesiveness of flagelliform silk originates from the application of an aqueous glycoprotein "glue" coating the core flagelliform silk fibre. The flagelliform core fibre and the applied sticky coating are two separate proteins produced in different glands and synthesized individually. Hygroscopic components in the glycoprotein glue attract water from the environment. The water keeps the glycoprotein and silk fibres of the web hydrated. Hydration of native flagelliform silk by the aqueous glue has been shown to supplement extensibility. Water naturally

plasticises silk proteins and thus plays a critical role in the mechanical properties of native silk fibres. Regenerated spider silk and chimeric spider silk-like fibres display improved mechanical properties when processed in aqueous alcohol solutions as such solutions plasticise the amorphous regions and promote secondary structural transitions that reorganize the fibre network (Hayashi & Lewis, 1998). Aside from the role of water, the strength and extensibility of spider silks has been correlated with the primary sequences of the proteins of the various spider silk fibres.

2.1.3. Recombinant spider silk

Due to the cannibalistic nature of spiders (Biotechnology & 2000, n.d.; Alexander Morin et al., 2016; F Vollrath, Polymer, & 2009, n.d.), it is extremely difficult to farm spiders for production of native spider silk. However, recent advances in producing recombinant silk protein have encouraged the further manufacture and application of this material (Schacht & Scheibel, 2014). The mechanical properties, biocompatibility and functionalization of recombinant silk by biotechnological methods has given rise to numerous silk based materials suitable for various biomedical applications such as implant coatings (Zeplin, et al., 2014), scaffolds for tissue engineering (Zhu, Li, Lewis, Segre, & Wang, 2015) (Lewicka, Hermanson, & Rising, 2012), wound dressing devices (Baoyong, Jian, Denglong, & Min, 2010) and drug delivery systems (J. G. Hardy, Leal-Egaña, & Scheibel, 2013; Lammel, Schwab, Hofer, Winter, & Scheibel, 2011).

There have been different approaches used to produce spider silk proteins recombinantly. Each method has its own pros and cons; however, the main focus has been to produce as long as repetitive spidroin region as possible. The first limitation is the difficulty in determining the complete cDNA sequence of the spider silk gene wherein inaccurate results provide us with limited information on gene size or the number of repeating units. Furthermore, sequencing of repetitive protein causes problem i.e. genetic instability deprived tRNA pools and undesired mRNA secondary structures as well as limitations related to the insolubility of the final product that may results in proteolysis (Zhou, Wu, & Conticello, 2001).

In order to overcome these difficulties, several approaches have been taken into consideration, such as codon optimisation, the expression of different genes and host systems. Prokaryotic and eukaryotic hosts such as bacteria, yeast, plants, insect cells, mammalian cells, and even transgenic animals have been tested. Each method has its

own limitations considering production cost and simplicity, expression levels and risk of host derived contaminations (Widhe M. , Johansson, Hedhammar, & Rising, 2012).

For instance, gram negative enterobacterium *Escherichia coli* (E. coli) is widely used for silk gene expression in large scale production, however it is complicated by different codon usage, unstable DNA fragments, insolubility and low protein yield (Römer & Scheibel, 2008). Other methods also suffer from various operational shortcomings. Gram positive bacterium protein secretion is simple, but limited in terms of genetic manipulation when compared to gram negative E.coli, and furthermore requires more precaution due to its pathogenic nature. Yeast can produce longer proteins with minimized truncation; however, unwanted glycosylation may induce specific immune responses in animals. Expression of the spidroin gene in plants like potato, tobacco allow for cheaper and more efficient protein production, but lower yield and possible traces of toxic substances can cause allergic reactions. There are several reports on the physical and biological regulation of neuron regenerative growth and network formation on recombinant dragline silks in various hosts (An et al., 2015; Markus Heim, Römer, & Scheibel, 2010; Jones et al., 2015; F Teulé, Cooper, Furin, protocols, & 2009, n.d.). Gene expression in mammalian cells offers closest human like condition; yet recombinant silk is relatively small (65-120 kDa compared to native >250 kDa) (Harris, et al., 2016). Mammalian cell lines are also prone to infections. Furthermore, the spider silk gene has been expressed in the milk glands of transgenic goats and mice, while the initial results were promising, lower concentrations of soluble protein in the milk prohibited further efficient purification for thorough analysis (Römer & Scheibel, 2008).

The expression and production of spidroin is followed by purification, artificial spinning and processing into solid structures (Widhe M. , Johansson, Hedhammar, & Rising, 2012). Self-assembly of recombinant silk takes place by dehydration or solvent removal to increase stability and β-sheet content, however, aqueous forms of recombinant silk can be processed to different mechanically, chemically and thermally stable scaffolds such as fibre, mesh, film and foam. After processing the proteins, they are usually treated by sterilisation techniques such as autoclaving, filtration or with alcohol or an aqueous solution of kosmotropic salts (e.g. potassium phosphate) to induce β-sheet formation in the material (Schacht & Scheibel, 2014).

2.2. Silk composites

The comprehensive review of Hardy and Scheibel (2010) (J. Hardy, Science, et al., n.d.) describes several processing methods for the manufacture of pure silk into films, foams, hydrogels, capsules, spheres and fibres. Silks may alter the morphology of crystallising calcium carbonate (Chen, Shao, & Vollrath, 2006), since the amino acid-based building blocks of silk position themselves between the crystallising segments, thus controlling the pattern of crystal growth and the final polymorph. In such cases, pure silks are foremost dissolved in concentrated solutions of inorganic or organic salts, in fluorinated solvents, ionic solvents or strong acids. Through dissolution, the hydrogen bonds are broken and the silk proteins are denatured. However, dissolution also allows the silk to be manufactured into a range of different structures. Manufacturing methods may include hand drawing, wet or dry spinning and electrospinning for the creation of fibres. Films may be formed through dip coating or spin coating, while hydrogels can be manufactured by exposure to an aqueous solution of polyethylene glycol (PEG) (Mw 8,000 to 10,000) solution (25-50 wt. %), Freeze drying such hydrogels gives rise to silk foams. Other methods for producing foams from silk hydrogels include gas foaming and salt leaching. Silk capsules are formed by adsorption of silk proteins to water in water–oil emulsions and silk spheres by electro spraying or precipitation reactions. Dissolution destroys the β–sheet proteins, however post–manufacturing treatment with alcohol or potassium phosphate encourages β–sheet proteins to reform (Fu, Shao, & Fritz, 2009b; J. Hardy, Römer, Polymer, & 2008, n.d.; J. Hardy, Transactions, & 2009, n.d.), thus recreating nanocrystalline reinforcing segments.

2.3. Bacterial cellulose

Cellulose, the most abundant organic compound on earth, is a structural component of plant and algal cell walls(Ansell & Mwaikambo, 2009; Horton, 2010; Siró & Plackett, 2010). Some animals, such as tunicates, as well as several bacteria, nevertheless also produce it. Natural cellulose has a crystalline and linear polymer along with an amorphous section. (Siro & Plackett, 2010) (Quiroz-Castañeda & Folch-Mallol, 2013). Cellulose is made of parallel unbranched D-glucopyranose units linked by β-1,4-glycosidic bonds that form crystalline and highly organised microfibrils through extensive inter and intramolecular hydrogen bonds and van der Waals forces. Amorphous cellulose exists where these bonds are broken and the ordered

arrangements are lost. Cellulose chains aggregated into microfibrils are reported to consist of 24 to 36 chains based on scattering data and information about the cellulose synthase (Quiroz-Castañeda & Folch-Mallol, 2013). Bacterial cellulose prepared from pellicles of *Acetobacter xylinum* is a unique biopolymer in terms of its molecular structure, mechanical strength and chemical stability (George, Ramana, …, & 2005, n.d.).

Bacterial cellulose has considerable potential in biomedical applications due to its high strength in the wet state, its moldability in situ, its biocompatibility and its relatively simple and cost-efficient production. Bacterial cellulose-based composites have been used for biomedical applications such as bone tissue engineering, blood vessels, wound dressings and cartilage replacement (Svensson, et al., 2005) (Czaja, Young, Kawecki, & Brown, 2007). Advantages in using bacterial cellulose over cellulose from other sources and polymers include; ease of processing to 3D shapes, networked fibre architectures and the ability to manufacture composites within the culture medium (Torres, Commeaux, & Troncoso, 2012). Mendes et al (Mendes, et al., 2009) tested the biocompatibility of implanted membranes made from bacterial cellulose on mice and confirmed a low inflammatory response that makes it suitable as a scaffold for stem cells. Bacterial cellulose is also designed for specific biomedical application. Spaic et al (Spaic, Small, Cook, & Wan, 2014) oxidised and aminated bacterial cellulose to produce pH sensitive hydrogels, which can be used for controlled drug delivery. Wanna et al (Wanna, Alam, Toivola, & Alam, 2013) and Veliz et al (Véliz, Alam, Toivola, Toivakka, & Alam, 2014) reported faster blood clotting times and higher blood attachment strengths by adding kaolin nanoparticles at the expense of losing mechanical strength. Furthermore, many have emphasised the importance of increasing biocompatibility and enhancing the material for specific application. There are various in determining mechanical performance of BC, Ul-Islam et al (Ul-Islam, Shah, Ha, & Park, 2011) reported c.a. 30% increase in the elastic modulus of BC that incorporates chitosan. Silica (Yano S. , Maeda, Nakajima, Hagiwara, & Sawaguchi, 2008), cellulases (Hu & Catchmark, 2011), starch (Wan, et al., 2009) and hydroxyapatite (Grande, Torres, Gomez, & Bano, 2009) are other biomaterials used to form composites with bacterial cellulose where the biocompatibility of bacterial cellulose has been modified. However, the mechanical performance of these materials has never been significantly improved. There are reports (Marsano, 2007) (Songmin Shang, 2011) (Yasutomo Noishiki, 2002) on silkworm silk fibroin composite with

cellulose which primarily aim to improve the mechanical properties of BC composites, however there is little to no work on combining spider silks and the amino acids they are built up from with (bacterial) cellulose.

3. Materials and methods

3.1. Bacterial cellulose preparation

Bacterial cellulose was extracted from nata (Bantul, Indonesia). The nata was initially boiled in water and drained thrice in order to remove basic chemical impurities and acetic acid from the culturing process. Following this, it was treated with caustic soda solution and then stored in freezer at -18°C. Prior to use, it was washed and crushed using a hand mixer and the resulting gel was treated with 0.1 M NaOH solution at 80°C for 20 min in order to purify the bacterial cellulose of microorganisms and residues from the media. The gel was subsequently neutralised by rinsing in deionised water after which it was filtered using a Buchner filtration funnel to increase the solids content c.a. 10% (Wanna, Alam, Toivola, & Alam, 2013).

3.2. Addition of amino acids as bio-glues to bacterial cellulose

Amino acid monomers were purchased from Sigma Aldrich in powder form. Samples were prepared by mixing 1.7 g of solid bacterial cellulose with different weight fractions of alanine and glycine. The mixture was poured into a rectangular pressure filtration unit and 1 MPa pressure was applied to manufacture composite sheets of c.a. 200 mm thicknesses. Leaching of amino acid from the bacterial nano-cellulose sheet was considered by weighing the amino acid residue in water expelled from the pressure filtration unit. The sheets were then dried in an oven at 80°C for 4 h. Six samples with different weight percentages were made using 0.1 g of alanine and glycine powder for BC-Ala and BC-Gly 95-5 weight fraction (W_f), and 0.425 g and 1.7 g for 80-20 and 50-50 BC-Ala and BC-Gly weight fractions respectively. BC-Pro composites were manufactured only using the weight fraction of 0.425 g for an 80-20 weight to weight composite.

Density was determined by measuring the thickness, widths and lengths of rectangular cuts of the material (to determine volume), drying the samples and then weighing them. We measured a total of nine samples for each material type.

3.3. TEMPO-mediated oxidation of bacterial cellulose

The TEMPO-mediated oxidation of bacterial cellulose was carried out in a reactor shown in Figure 5 following the method published in (Huang, Chen, Jiang, & Li, 2013) (Shinsuke Ifuku, 2009); initially bacterial cellulose sheets (0.648 g solid, i.e. 4 mmol of

anhydroglucose units) was dispersed in a Na_2CO_3/$NaHCO_3$ buffer solution (80 ml, pH = 10). After quick dispersion with moderate stirring, the reactor was placed in ice bath to take the reaction to 0ºC, and TEMPO (10 mg, 0.065 mmol) and NaBr (0.20 g, 1.9 mmol) were added to the suspension. To start the reaction, sodium hypochlorite solution, which was stored at 0ºC (21%, 4.10 ml, 13.20 mmol), was added to the reactor and the pH was adjusted by 0.5 M aqueous NaOH to 10. The reaction was stirred overnight and finally the oxidation was quenched by adding 10 ml of methanol. The oxidized cellulose was precipitated by adding five volumes ethanol, rinsed with ethanol/water solution, centrifuged several times, and dialysed in distilled water overnight. The product was then dried at 65ºC.

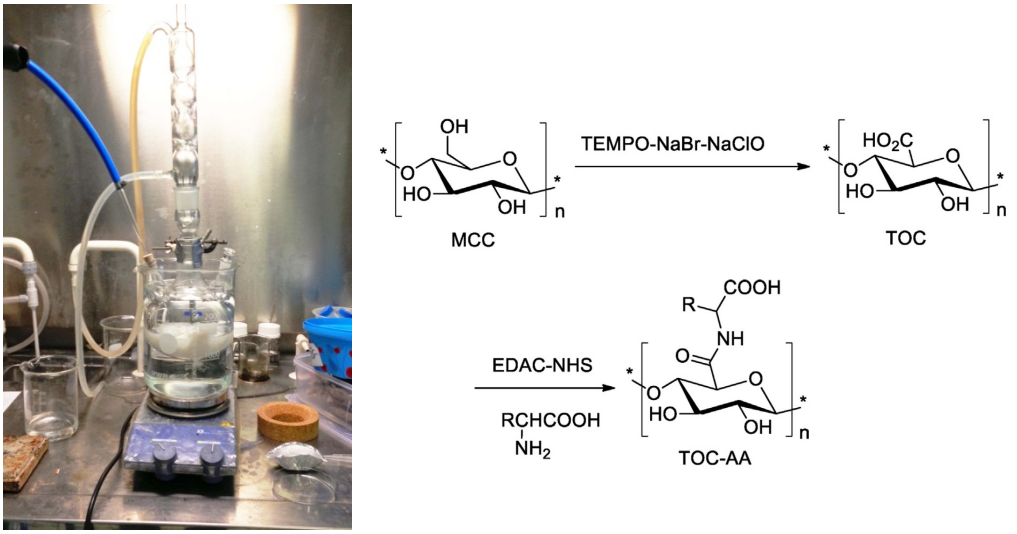

Figure 5 – (a) Synthesis reactor for TEMPO-mediated oxidation of bacterial cellulose and (b) schematic illustration for the preparation of amino acid modified TEMPO-oxidized cellulose

The grafting of amino acids to oxidised cellulose was carried out by following a method described in (Huang, Chen, Jiang, & Li, 2013). 10 mg of dried oxidised bacterial cellulose was initially added to 50 ml of deionized water. The mixture was stirred in the reactor under moderate magnetic stirring to form a homogeneously dispersed solution, after which 23 ml of N-hydroxy-succinimide (NHS) aqueous solution (50 mg ml−1) was added. 12 ml fresh N-ethyl-N-(3-dimethylaminopropyl) carbodiimide hydrochloride (EDAC) aqueous solution (10 mg ml−1) was added to

the suspension and stirred vigorously for 30 minutes at room temperature. The pH was adjusted to close to neutral by adding NaOH or HCl. The excess EDAC, NHS and by-product urea were removed by dialysis in distilled water for 8h. Finally, 100 mg of glycine, alanine and proline was added to 100 ml of suspension and later dialysed to remove un- reacted amino acids and other residues over a period of 2 days. The final product was partially dried and was later pressure filtrated to form composite sheets for further tests.

3.4. Manufacturing composite materials

Pressure filtration was used to manufacture various composites samples. The custom build pressure filtration rig uses a similar principle to ordinary pressure filtration rigs used to prepare samples for mercury porosimetry (Cathy J. Ridgway, 2011; Touaiti, et al., 2013), and utilises a filtration pressure of 1 MPa. The samples were prepared for FTIR spectroscopy and tensile tests.

The pressure filtration rig is constructed from three aluminium parts (see Figure 6). The upper part includes a nozzle through which compressed air is injected and the middle is moulded with a rectangular 120mm long and 80mm wide chamber. The lower aluminium part was drilled with holes in order to allow water to be squeezed from the composite mixture and to exit the rig. The holes are around 1mm in diameter; however, a porous polycarbonate membrane with a pore dimeter of 30 nm was used just to allow the excess water to pour easily out from the mould. To protect the membrane from the pressure applied on the mixture, a metallic mesh was inserted beneath the membrane as a support.

Composites were prepared initially by mixing the constituents with a specific percentage. The mixture was poured into a pressure filtration unit and 1 MPa pressure was applied. The desired thickness of sheets was 200 μm which was achieved by adding 1.7 g of solid bacterial cellulose, though the thickness might vary up to 30% in different samples. The sheets were taken out of the pressure filtration rig after 5 hours and then dried in an oven at 70°C for 5 hours, after which it was left at room temperature.

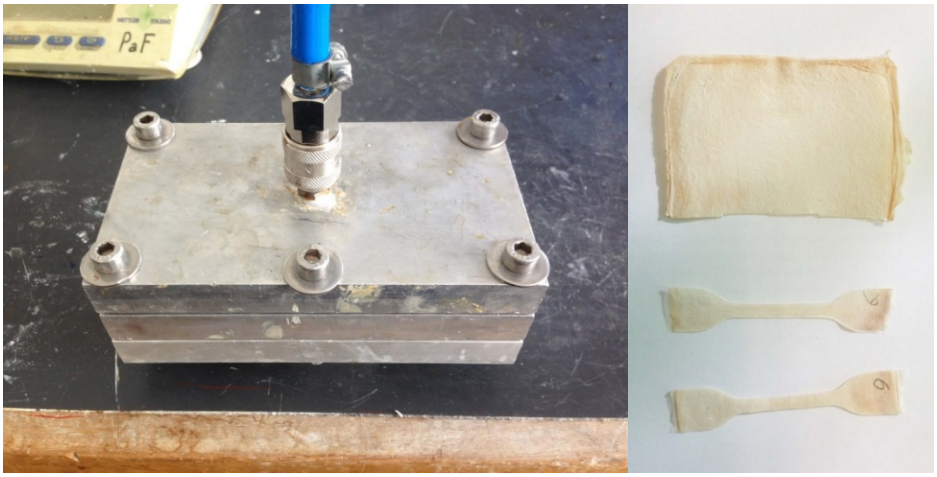

Figure 6 – Pressure filtration rig on the left and prepared sample with cut out dog-bone shape sample for tensile testing on the right

The samples were cut into dog-bone form with a gauge length of 50 mm and a width of 4 mm. The exact thickness of each sample was also measured using a digital micrometre.

3.5. FTIR spectroscopy

FTIR spectra were identified using a Perkin Elmer Spectrum One equipped with an ATR-FTIR unit. A small sample from each composite was placed on a crystal (diamond/ZnSe). The spectra were obtained with a resolution of 4 cm^{-1} and with 128 scan iterations, at a wavelength range of 650–4000 cm^{-1}. The spectra were collected and analysed using Spectrum software (Perkin Elmer).

3.6. Mechanical testing

The mechanical properties of composites were ascertained using an Instron 8872 (with a 1.5kN load cell). The tests were performed on dog-bone shaped samples cut from each composite sheet. 5 dry samples and 5 wet samples were tested from each composite sheet. Wet samples were placed in a humidity chamber at 30°C and 90% relative humidity for 5 hours and tested immediately after removal from the chamber. Tensile tests were performed at crosshead speed of 1mm/min, under room temperature conditions of 25°C ± 2°C and a relative humidity of 55 %.

3.7. Computational modelling

Detailed atomic level simulation is indispensable for complicated mechanisms like protein folding and for providing molecular mechanistic insights where such information cannot easily be obtained through experimentation (Caflisch & Paci, 2005) (Shea & Brooks III, 2001). Ascalaph Designer (v1.8.90) was used to model the self-assembly and determination of intermolecular interaction of designed samples. The software has pre-defined quantum mechanical calculations for charge distributions in amino acids and proteins. Furthermore, Firefly (v8.1.1) (Granovsky, n.d.) was used for quantum mechanical calculations to predict the charge distributions of bacterial cellulose and other components such as modified BC.

Simulations were run on small scale models, due to computation power limitation to handle modelling of large molecules. However, our model were designed to simplify the understanding of the intermolecular behaviour and the subsequent effects this has on molecular structure, energy and mechanical properties. Intermolecular and potential energy of each model were recorded during material relaxation process. The temperature was kept constant at 298.15 K and the time per step was set at 0.1 femtoseconds for all simulations.

In the first modelling study, single MaSp1 strands containing 8 and 12 poly-Ala β-strands and single MaSp1 strands containing 'double β-strand' groups equally segmented and spaced with 4 and 6 monomers were constructed. The amino acid sequence used for MaSp1 is inspired from original MaSp1 protein sequence (Bratzel & Buehler, 2012a) and our designed model is shown in Table 4a. Two adjacent protein strands were aligned at a distance of 10 Å and subjected to energy minimisation [30] prior to folding.

For BC composite with flagelliform silk and separate amino acids, two adjacent strands with 36 anhydroglucose units of bacterial cellulose $(C_6H_{10}O_5)n$ were aligned at a distance of 15Å. The space with two BC strands was filled with various materials of flagelliform silk, monomeric glycine, alanine and proline and BC strand for reference. The modelled flagelliform silk was inspired from native flagelliform silk (M Heim, Ackerschott, biology, & 2010, n.d.) and shown in Table 4b. This sequence contains the predominant repeating units of flagelliform silk; GPGGX and GGX. The

molecular weight of the free amino acids and reference bacterial cellulose were kept the same as the flagelliform silk protein.

Table 4 - List of a) MaSp1 and b) flagelliform protein sequences modelled (An, GGX and GPGGX repeating units are highlighted in green, blue and yellow respectively).

a)	
8 alanine groups	GGAGQGGYGGLGSQGAGRGGLGGQGAAAAAAAAGGAG QGGYGGLGSQGAGRGGLGGQGAG
12 alanine groups	GGAGQGGYGGLGSQGGLGGQGAGGAAAAAAAAAAAG QGGYGGLGSQGAGRGGLGGQGAG
2×4 alanine groups	GGAGQGGYGGLGGAAAAGGAGSQGAGRGGLGGQGAGG YGGAAAAGAGRGGLGSQGGQGAG
2×6 alanine groups	GGAGQGGYGGAAAAAAGGAGSQGAGRGGLGGQGAGGY GGAAAAAAGGRGGLGSQGGQGAG
b)	
Flagelliform silk	GGA GPGGA GPGGV GPGGS GPGGY GPGGA GGA GGS GPGGAGGPY GPGGS GPGGV GPGGA

Lastly, three adjacent molecules of bacterial cellulose with grafted amino acids were positioned in parallel with an initial separation distance of 10Å. Each molecule consisted of 36 glucopyranose repeats and 12 amino acids. Glycine, alanine and proline were attached to the C6 primary carboxyl group, to mimic the TEMPO-oxidised amino acid covalent grafting from the experimental work.

In all models, simulation starts from an extended state. To perform folding simulations of strands to their equilibrium states of lowest energy (folded conformations) we employed molecular dynamics methods using an AMBER94 force field, the basis of which is shown in Equation 1. In this force field, four terms define the potential energy of the system; the first and second terms include the energy of covalently bonded atoms and their angles respectively, which are represented by harmonic potentials near the equilibrium bond length. A third term is for torsion, which is represented by a Fourier series. The last term refers to non-bonded energy between all atom pairs, which consists of van der Waals and electrostatic forces. These are based on 6-12 potentials and Coulomb's law respectively (Cornell, et al., 1995).

$$E_{total} = \sum_{bonds} K_r\left(r - r_{eq}\right)^2 + \sum_{angles} K_\theta\left(\theta - \theta_{eq}\right)^2 +$$

$$\sum_{dihedrals} \frac{V_n}{2}\left[1 + \cos(n\varphi - \gamma)\right] + \sum_{i<j}\left[\frac{A_{ij}}{R_{ij}^{12}} - \frac{B_{ij}}{R_{ij}^{6}} + \frac{q_i q_j}{\epsilon R_{ij}}\right]$$

Equation 1 – Equation defining the force field **(Cornell, et al., 1995)**, where K_r is determined by linear interpolation between pure single and double bond values, r and r_{eq} represent the calculated and equilibrium bond distance, K_θ is determined from vibrational analysis of a simple sp^2 atom, θ and θ_{eq} are bond angles. V_n represent the magnitude of torsion and φ and γ are sinusoidal parameters of torsional rotation curve. Lastly, A and B parameters control the depth and position of the potential energy for non-bonded interacting atoms.

Furthermore, VMD Visual Molecular Dynamics (v1.9.2 beta1) (Humphrey, Dalke, & Schulten, 1996) was used to visualize molecules and detect the hydrogen bonds in the simulated molecules.

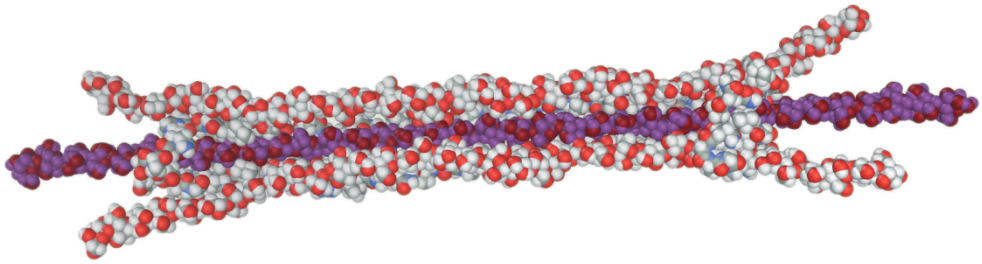

Figure 7 – Example model for bacterial cellulose molecules interacting with flagelliform silk molecules

4. Summary of results

4.1. The effects of electrostatic charge on molecular toughening in MaSp1 (spider silk) proteins

The molecular structure of MaSp1 silk is highly dependent on the chemical structures of its constituent proteins within the silk glands, as well as mechanical factors such as reeling speed and shear stresses during the drawing of the silk thread (Chen, Shao, & Vollrath, 2006) (Vollrath & Knight, 2001). The process of self-assembly instigates formation of the secondary structure of the protein. Dudley and Ortega-Jimenez (Ortega-Jimenez & Dudley, 2013) investigated the deformation of spider webs caused by electrostatic charges in favour of increasing the chance of prey capture. Positively charged surfaces of insects are able to rapidly attract of silk threads.

To further investigate the effect of electrostatic attraction on spider silk, we designed a model with two adjacent MaSp1 proteins with specific size and spacing of A_n units. Under a non-contacting electrostatic pulling force, the deformation mechanisms of MaSp1 protein were investigated. Here, the interaction of hard and crystalline A_n units with respect to soft and amorphous GPGXX units, GGX units and spacers were considered in the deformation of MaSp1 silk proteins. The models consist of various sizes and spacings of crystalline A_n unit to characterise the folding mechanism of MaSp1 protein molecules to an energetic equilibrium steady state from their initial state after extrusion (Cranford & Buehler, 2010). Furthermore, folded MaSp1 strands were subjected to electrostatic pulling forces and the resultant elongation was investigated.

The crystalline segments of MaSp1 are a few nanometres in length and constitute at least 10–15% of the silk volume (Fu et al., 2009b; J. Hardy, Römer, et al., n.d.; Römer & Scheibel, 2008). In order to have a mechanically stable β-sheet, an A_n segment should consist of at least 6 alanine units. This relates to the zipping mechanism of β-sheet stacks and there is no distinctive improvement beyond 8 monomer units (Bratzel & Buehler, 2012b). Therefore, we designed 4 samples; two with long 8 and 12 units of alanine located at centre of a molecule and two samples with two shorter A_n segment located equidistant from the centre leaving an amorphous central region. The self-assembly process was initiated from an elongated and aligned molecular state.

Results from the self-assembly process reveal that two-molecule MaSp1 strands with segmented crystalline sections fold to considerably shorter lengths when compared to strands with single crystalline segments. In Figure 8, changes in the total length of the adjacent protein strands, both crystalline and amorphous parts were monitored as a function of time. The length of the crystalline regions of the two-molecule strand do not change dramatically and they reach steady state at shorter times as they have lower free energies and lower mobilities as compared to the amorphous segments. The amorphous regions fold considerably more and a longer time is required for these regions to reach steady state. In the samples with two shorter crystalline sections, the amorphous site between crystalline sections was observed to fold more. Furthermore, they reached steady state over a longer period of time and exhibited lower intermolecular energies. The amorphous regions at head and tail of the strands were not constrained from both ends, therefore they had more freedom to fold into their preferred configurations. The intermolecular energy ΔE_T and the time required for the samples to reach their stable folding configurations are listed in Table 5.

Table 5 – ΔE_T values indicating conformational stability in the folded state. Times (fs) to reach steady state are also provided for each of the modelled MaSp1 types.

Type	ΔE_T (Kcal/mol)	Time (fs) (Steady State)
2×4 Alanine	-981	107
8 Alanine	-862	78
2×6 Alanine	-1184	118
12 Alanine	-965	93

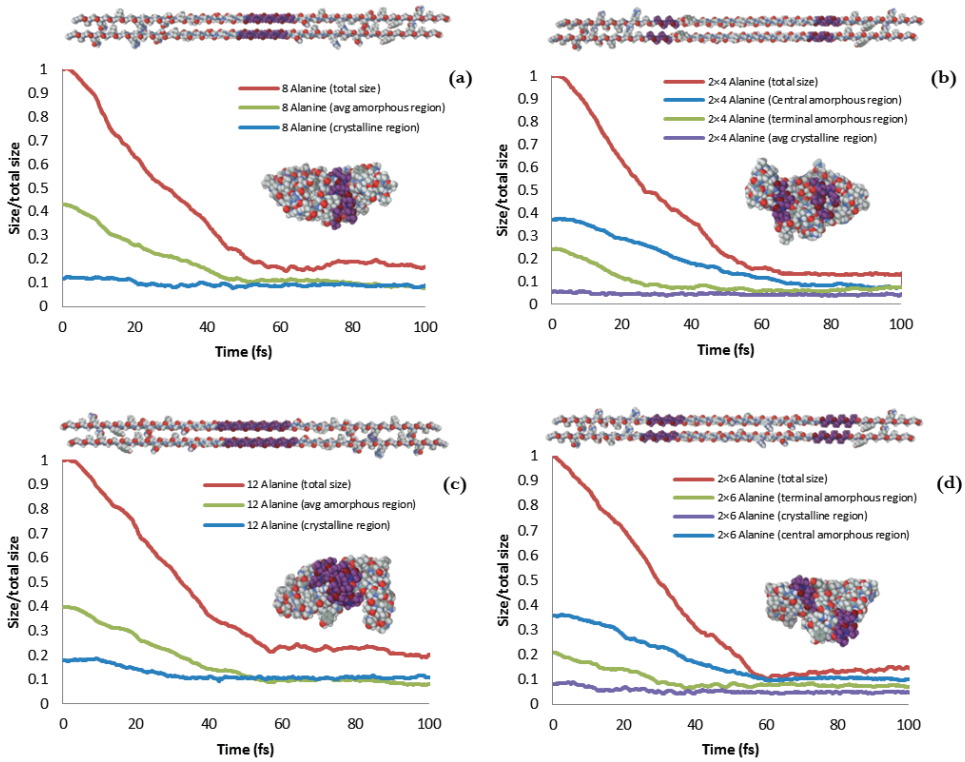

Figure 8 – Variations in the distances between terminal atoms for different regions of MaSp1 strands during the folding process; for silk proteins with crystalline region of (a) 8 alanine groups, (b) 2×4 alanine groups, (c) 12 alanine groups and (d) 2×6 alanine group. The extended and folded conformations are shown in each case.

Two folded adjacent strands of MaSp1 in the model undergo four different stages of deformation when they are subjected to an electrostatic pull. These stages have been previously reported by Cranford and Buehler (Cranford & Buehler, 2012), but for mechanical pulling force. When a force is applied, the folded strands show an initial resistance (I), wherein weaker hydrogen bonds in the amorphous section are breaking. The second stage, corresponds to resistance due to entropic unfolding of amorphous region (II). In the next stage, there is a significant rise in the resisting force from crystalline β-sheet sections that requires the breaking of the network of hydrogen bonds (III). The last stage involves frictional resistance to sliding and self-healing that may occur during sliding (IV). The force-strain curve diagram of unfolding

mechanism of 8-Ala MaSp 1 (single β-sheet) at electrostatic pull of +76.8 aC, has been depicted in Figure 9.

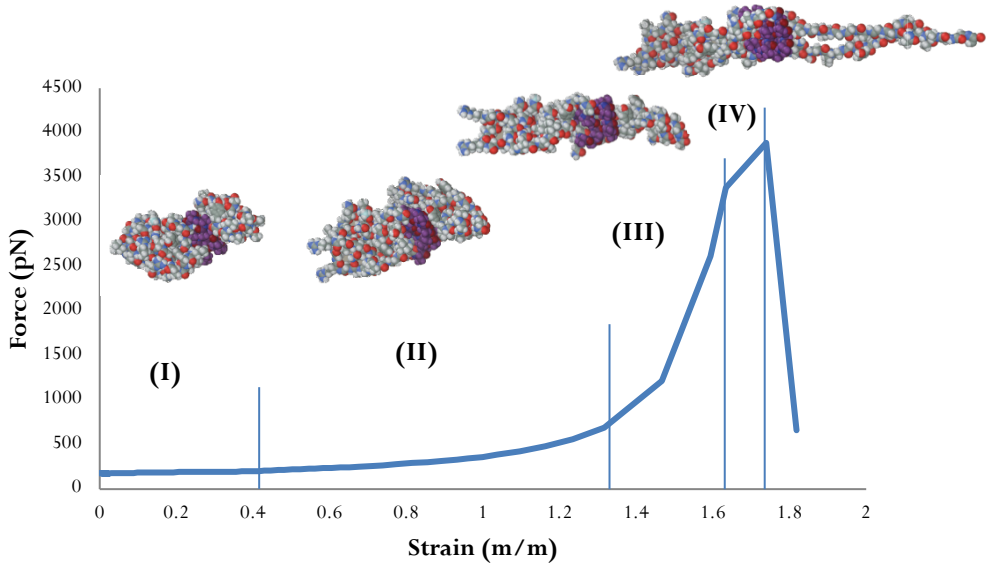

Figure 9 – Schematic stress-strain curve for deformation of two adjacent silk protein, the curve is depicted for folded MaSp1 proteins with 8 alanine groups with dummy charge of +76.8 aC

The main resistance in the third stage is related to hydrogen bonding, interlocking and a self-healing mechanism in the crystalline section. Alanine and glycine are the main constituents of MaSp1 proteins and alanine contribute primarily to the formation of β-sheet nanocrystals. Alanine has a high affinity to form hydrogen bonds on both sides of the molecule, and while the β-sheet stacks are sliding over one another under a pulling force, the continued possibility for H-bond formation and physical obstructions caused by methyl groups on the side chains provide increased resistance. Nevertheless, when reaching a glycine group, a lack of any methyl groups leaves 'holes' (Lewis, 2003) on the side of each motif, which lowers the resistance to shear, Figure 10.

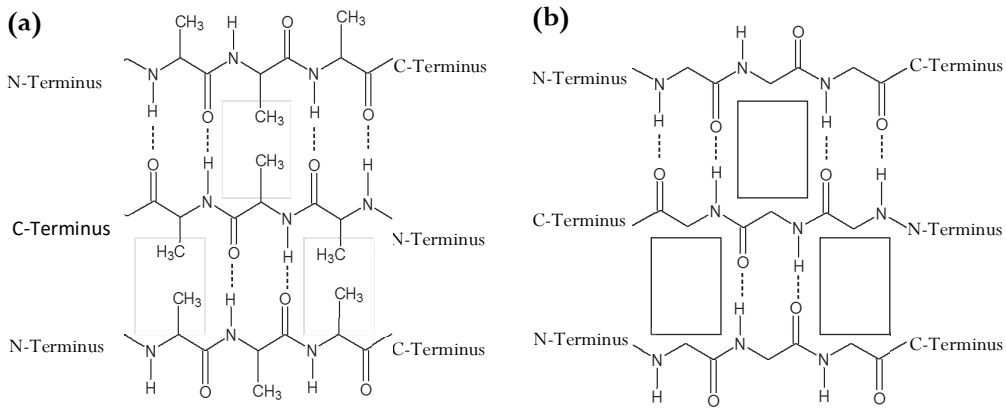

Figure 10 – Antiparallel alignment of β-sheet crystals formed by (a) alanine groups and (b) glycine groups, the box shows the holes in glycine β-sheet which makes it weaker that alanine β-sheet. Other amino acids may form β-sheet but bigger side chains hinder the creation of strong β-sheet crystals.

In our model, each sample was subjected to a different electrostatic pull which in turn was adjusted by altering the surface charge of a pulling point. The range of force to failure in this model was in agreement with a previous study (Keten & Buehler, 2010b) wherein mechanical shear forces were employed and the force to failure for a similarly sized molecular model was reported at around 2300 pN. The force to failure, strain to failure and the time required for each simulation are provided in Table 6. From Table 6, MaSp1 molecules with segmented poly-Ala chains show a superior mechanical performance as compared to MaSp1 proteins with single crystalline sections. In protein strands with segmented crystalline sections while sliding under electrostatic pulling force, the poly-Ala section can temporarily recreate β-sheets with the second poly-Ala site of a neighbouring strand. This 'second catch' mechanism increases the required energy for mechanical deformation.

The crystalline segments of MaSp1 in our simulations are beyond the critical 'zipped' length of ca. 3 monomers (Bratzel & Buehler, 2012b). Essentially, the smallest β-strands modelled are close enough to their stress transfer aspect ratio (Hull & Clyne, 1996), are sufficiently 'zipped' (Bratzel & Buehler, 2012b), and are able to withstand load. Indeed, the synthesis of poly-alanine regions longer than 8 alanine groups is

metabolically expensive and poly-Ala segments larger than this are atypically long (Craig, Hsu, Kaplan, & Piercea, 1999).

When silk proteins are stretched, the β-sheet crystals will orient to the direction of loading and reinforce the partially extended fibre. They improve cohesion between the long polypeptide strands, enabling the amorphous domains to stretch more extensively. The total folded length of the strand containing two crystalline segments tends to be smaller than the strand containing one longer crystalline segment, and this also exhibits a higher strain to failure than the single crystal protein couplings. We suggest the mechanism underlying this phenomenon relies very much on the 'concertina-like' role of the amorphous segments. In the two-crystal systems, three amorphous sections are unfolding simultaneously until the soft matter is completely unfolded. This results in a higher strain and the faster elongation of the protein strand. Failure occurs when unfolding is complete, and the load is transferred to the crystalline section where hydrogen bonds are then able to break.

Table 6 – Failure forces, strains and times for the different silk proteins modelled and under the influence of different electrostatic pulling forces.

Type	Electrostatic pull (aC)	Force at failure (pN)	Strain at failure (m/m)	Time (fs)
2×4 Alanine	+51.2	2328	2.01	8.2
	+76.8	3916	2.00	5.8
	+102.4	4925	2.00	5.0
8 Alanine	+51.2	2245	1.64	20.6
	+76.8	3233	1.85	14.0
	+102.4	3887	1.74	9.3
2×6 Alanine	+51.2	1467	2.79	9.5
	+76.8	3316	2.74	7.9
	+102.4	4735	2.77	6.5
12 Alanine	+51.2	1252	1.34	17.5
	+76.8	3124	1.27	11.5
	+102.4	4821	1.37	9.9

4.2. Bacterial cellulose nanocrystals as alternatives to MaSp1 nanocrystals

The concertina-like mechanism of MaSp1 is the outcome of a combination of stiff nanocrystalline structures of β-sheets and amorphous 3_1 helical structures of glycine rich amorphous matter. To mimic this structural mechanism, we considered bacterial cellulose as it is a material with high crystallinity. Bacterial cellulose prepared from bacterium such as *Acetobacter xylinum* has ca. 95% crystallinity, however these crystals lack the extensibility of MaSp1 proteins. Flagelliform silk has a high extensibility and might be a potential additive to bacterial cellulose, by which means the stretch of a BC based material could be increased. We hypothesised that by the addition of flagelliform silk to BC, similar characteristics to MaSp1 may be achievable, thereby toughening BC sheets. We therefore modelled BC-Flag combinations to better understand their interaction behaviours and global mechanical properties.

4.2.1. Flagelliform silk composite with bacterial cellulose

Flagelliform silk is the main constituent of the capture spiral and benefits the web in that it has a super elastic structure. This structure is able to dissipate high impact energy and stretch up to 4 times of its original length. The initial resistance against load comes from a weak network of intramolecular hydrogen bonding from within the β-spirals. This spring shape spiral opens up to bear higher shear forces, however it lacks β-sheet stacks and this aspect limits its strength. The flagelliform silk protein sequence is highly repetitive and consists of mainly GGX and GPGGX repeating units. The mechanical behaviour of flagelliform silk has inspired us to study its adhesive properties in BC based composites. Unlike silkworm silk, there are limited reports on composite material comprising spider silk proteins. Here, we aim to elucidate the important features of flagelliform silk that make it an elastic bioglue. We subsequently employ some of these features to develop simpler (free amino acid) bioglues for BC biomaterials with an ultimate objective of mechanical enhancement.

4.2.2. Molecular dynamics simulations

Molecular dynamics methods were employed to investigate the adhesive mechanism in flagelliform silk when applied as an additive in a BC composite. It was hypothesised that the crystalline structure of bacterial cellulose containing flagelliform silk proteins might exhibit high strength (from the cellulose) and improved extensibility (from the

flagelliform silk molecules), leading to improved mechanical toughness. Bacterial cellulose withstands the initial load while the flagelliform silk molecules extend. When flagelliform silk is stretched, it can also interact with bacterial cellulose by creating hydrogen bonds. The extent of hydrogen bond formation within the composite structure at the molecular level determines the adhesion.

In this model, flagelliform silk was placed between two adjacent bacterial cellulose strands with 36 units of cellulose. The molecular structure of modelled flagelliform silk was shortened from natural flagelliform silk to 60 amino acid units containing the major GPGGX and GGX repeating units. This model was designed to mimic chemical and mechanical characteristics that natural flagelliform silk would have (M Heim et al., n.d.). Flagelliform silk consists of mainly glycine, alanine and proline in the amounts of 47%, 12% and 12%, respectively. The protein sequence of modelled flagelliform silk is presented in Table 7.

GPGGX and GGX repeating units form β-turns and 3_1 turn in secondary structure respectively during the process of self-assembly, eventually crimping to a spring like helicoid. These spirals are intramolecularly connected by a network of hydrogen bonds and are highly crimped. However, the structure is considerably weaker than that of β-sheets in dragline silk. Figure 11 reveals the extended and relaxed state of modelled flagelliform silk.

In a composite based on bacterial cellulose, internal hydrogen bonding is important for providing adhesion between the composite components. This phenomenon can be seen also in monomeric amino acids. Glycine, alanine and proline are able to form hydrogen bonds with bacterial cellulose and have the added advantage of being more mobile than a long flagelliform molecule. This mobility of smaller monomeric amino acid molecules will result in greater potential for hydrogen bonding within a BC composite. Furthermore, under shear, these molecules will slide and re-create hydrogen bonds with neighbouring cellulose which increases the ability of the material to self-heal.

The molecular weight of the separate amino acids and reference bacterial cellulose were kept the same and aligned in the same fashion as with the flagelliform silk protein. Molecular dynamics simulations were performed in a vacuum, with an

implicit water Sheffield condition, a constant temperature and each iteration was set at 0.1 femtoseconds in all simulations.

Figure 11 – Spring effect of flagelliform silk when subjected to stress and release a) extended state and b) relaxed state. In its extended state, intermolecular H-bonds that normally keep the structure crimped are broken. These sites have become free to bind (H-bond) with BC chains, resulting in strong adhesion between the two.

Table 7 – Number of hydrogen bonds between molecules in the modelled samples and the intermolecular energy after self-assembly and at steady state

	Maximum number of H-bond	Average number of H-bond	Intermolecular Energy kcal/mol
Pure BC	56	41	-1512
BC-Gly	75	62	-1676
BC-Ala	84	66	-1771
BC-Pro	64	53	-1707
BC-Flag	81	64	-1696

The intermolecular energy of modelled samples is mainly based on hydrogen bonding and van der Waals interactions. Addition of Flag and monomeric amino acid to the

BC composite considerably increases the intermolecular energy of the system, hence these have a higher adhesive energy. Furthermore, BC-Ala forms slightly more hydrogen bonds as compared to BC-Flag and other monomeric amino acids, and BC-Ala moreover exhibits a higher intermolecular energy.

Alanine and glycine have similar molecular structures and both have a high potential for hydrogen bond formation, whereas the ring structure of proline inhibits hydrogen bonding. However, the large size of proline is compensated somewhat by higher increased van der Waals interactions. Figure 12 illustrates the chemical structure of BC-AA and the intermolecular interactions with bacterial cellulose strands. The results from the molecular dynamic simulations confirm that the higher mobility of monomeric amino acids and the ability to form hydrogen bond compensates for the lack of a spring-like contribution that is observed in a flagelliform silk molecule additive to BC. Here, higher mobility provides higher malleability, better ease of repositioning, better movement and more stable H-bonding which consequently contributes to self-healing and energetic stability. Therefore, mobile amino acid bioglues in combination with crystalline BC is able to behave mechanically, in a similar way to BC-Flag. Furthermore, amino acids glycine and alanine have a comparable adhesive strength, but are more convenient to add to BC, are more easily acquired and are economically more viable than the harvesting of flagelliform silks. As such, we consider experimentally determining the actual mechanical benefits of gluing together BC strands with either alanine or glycine.

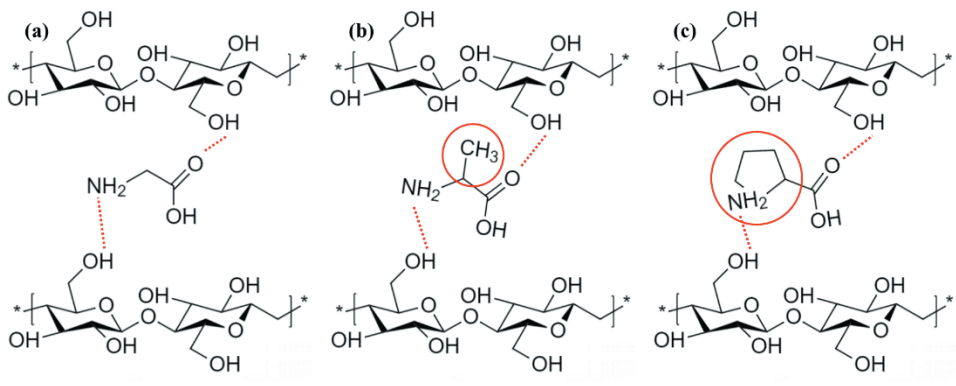

Figure 12 – H-bonding characteristics between BC (top and bottom molecules in each panel) and (a) glycine (b) alanine and (c) proline. In (b) we highlight the interlocking

side chain of alanine and in (c) we highlight the large ring of proline that hinders close range secondary bonding.

4.2.3. FTIR analysis of manufactured composites

The FT-IR spectra of our manufactured composites are shown in Figure 13. The main bands for bacterial cellulose are situated at 3340 cm^{-1} for OH stretching, 2893 for CH stretching in CH_2 and CH_3 groups, 1428 cm^{-1} correspond to CH_2 symmetric bending and 1162 cm^{-1} for antisymmetric bridge C–O–C stretching (Barud, et al., 2008). In the composite FT-IR spectra, COO^-, NH^{3+}, CH (Schulten, Dalke, & Schulten, 1996), CH groups are mostly considered to be assigned. In BC-Ala the carboxylic COO^- stretching wavenumber is in the range of 1680–1540 cm−1 (Barth, 2000) (Lydia Caroline, Sankar, Indirani, & Vasudevan, 2009), and there is peak at 1628 cm^{-1} indicating COO^- strong asymmetric stretching. The same peaks are assigned at 1635 cm^{-1} for glycine and proline (Mary, Ushakumari, Harikumar, Varghese, & Panicker, 2009; Reva, Stepanian, …, & 1994, n.d.). The intensity of C=O bands will increase due to the formation of hydrogen bonds (Lydia Caroline, Sankar, Indirani, & Vasudevan, 2009). Moreover, on the shoulder of the COO^- band, H-bonding is visible by de-convoluting the spectra in the range of 1610 cm^{-1} to 1620 cm^{-1} where there is strong peak at 1615 cm^{-1} corresponding to H-bonding. In amino acids containing NH^{3+} group, the stretching and bending vibrational wavenumbers are expected to occur in the regions 3150–3000 cm^{-1}, 1660–1610 cm^{-1} and 1550–1480 cm^{-1} (Lydia Caroline, Sankar, Indirani, & Vasudevan, 2009). The amine group peak in proline appears at 1539 cm^{-1} (Reva, et al., 1994), and in in alanine appears at 1520 cm^{-1}. Furthermore, clear peaks appear at 2852 cm^{-1} for proline indicating CH stretch that in our samples appear at wavenumber 2855 cm^{-1}.

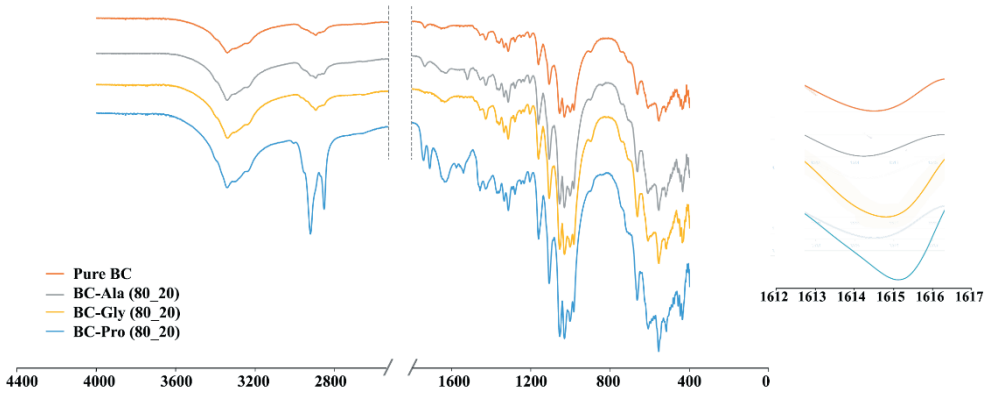

Figure 13 - (a) FTIR spectra for BC, BC-Ala (80-20), BC-Gly (80-20) and BC-Pro (80-20) and (b) H-bond peaks for each after spectral deconvolution

4.2.4. Mechanical properties of bacterial cellulose-amino acid composites

Mechanical tests were conducted using manufactured composite sheets detailed in sections 3.2 and 3.4. Table 8 provides the mechanical properties of tested samples in both dry and wet states. According to Table 8, BC-Ala samples with various weight percentages have superior mechanical properties when compared against BC-Gly and BC-Pro with respect to ultimate strength, elastic modulus and toughness.

BC-Ala composites show better mechanical performance as compared to the BC-Gly composite sheets. The BC-Ala composites surpass BC-Gly in ultimate strength and toughness, however it exhibits a lower elastic modulus. The higher malleability of glycine results in higher resistance compare to alanine within the elastic state. Glycine molecules are smaller and have a higher mobility, which increases the flexibility of composites at smaller loads. However, when increasing the load, due to its size, there are less collisions, van der Waals attractions and hydrogen bonds that form, resulting in a lower strength at failure and consequently a lower toughness as compared to BC-Ala samples. Contrarily, the higher hydrogen bonding density of alanine rich composites, which was confirmed by computational modelling, plays an important role in increasing the toughness of the composite sheet.

Table 8 – Mechanical performance comparison between different percentage of bacterial cellulose and amino acids composite

	Density (ρ) - kg/m^3	E/ρ - MNm/kg	σ_{ult}/ρ - kNm/kg	E/E (BC)	G/G (BC)	σ/σ (BC)
Pure BC	969	3.7	60.6	1.0	1.0	1.0
Pure BC_RH95		2.0	56.2	0.5	1.3	0.9
BC-Gly_(80-20)	747	8.0	112.9	1.7	1.1	1.4
BC-Gly_(80-20)_RH95		7.1	110.0	1.5	1.1	1.4
BC-Gly_(95-5)	999	5.1	74.0	1.4	1.0	1.3
BC-Gly_(95-5)_RH95		4.0	66.7	1.1	0.9	1.1
BC-Gly_(50-50)	1027	4.2	63.7	1.2	1.0	1.1
BC-Gly_(50-50)_RH95		3.8	59.7	1.1	0.9	1.0
BC-Ala_(80-20)	953	6.2	100.4	1.6	1.5	1.6
BC-Ala_(80-20)_RH95		4.6	79.5	1.2	1.2	1.3
BC-Ala_(95-5)	938	4.8	87.8	1.3	1.4	1.4
BC-Ala_(95-5)_RH95		2.4	64.9	0.6	1.2	1.0
BC-Ala_(50-50)	1013	3.8	63.0	1.1	1.3	1.1
BC-Ala_(50-50)_RH95		2.9	54.9	0.8	1.0	0.9
BC-Pro_(80-20)	998	3.2	61.7	0.9	1.2	1.0
BC-Pro_(80-20)_RH95		1.7	53.5	0.5	1.1	0.9

BC-Ala (80-20) composite samples are overall the strongest and toughest manufactured samples (Figure 14). The Young modulus of BC-Ala (80-20) is similar to that of BC-Gly (80-20), but it has higher toughness values in each of the equivalent fractions of BC-Ala samples. To the contrary on wet samples, BC-Gly (80-20) exhibit higher strength and toughness compare to BC-Ala samples, however BC-Ala composites have a comparatively greater toughness in the wet state. The phenomenon can be explained as glycine is more malleable molecule, with a higher mobility

compared to alanine. With a gap between the peptide linkage, glycine can more easily accommodate water molecules that leads to stronger and stiffer material compare to many other BD-AA composites in a wet state. Furthermore, unlike alanine, glycine has an ionic form in the presence of water molecules, which also potentially improves the mechanical performance of BC-Gly (80-20) in its wet state.

Based on our simulated models, alanine develops more hydrogen bonds with neighbouring cellulose strands than glycine. This moreover enhances the self-healing phenomenon as hydrogen bonds may reform when load is applied and the cellulose strands shear over one another. The extra methyl group in alanine improves self-healing by providing a physical block that increases the resistance of cellulose-shearing. Proline being the bigger molecule shows inferior strength and stiffness properties to alanine and glycine in BC composite. The large pentagonal ring of proline hinders secondary interactions and physically blocks BC from coming close enough to develop strong interactions with the amino acid.

The results from the mechanical tests show that an 80-20 mass fraction of bacterial cellulose with either alanine or glycine is superior in mechanical performance when compared to the 50-50 and 95-5 mass fractions. We suggest this is the result of molecular geometries within the composite. Here, low fractions of amino acid (5%) disrupt cellulose-cellulose interactions but offer no mechanical benefit, and high fractions of amino acid (50%) coat the cellulose molecules such that the amino acids interactions determine the global properties of the composite. The optimal fraction is an intermediate fraction where the amino acids make a contact layer between cellulose strands, but do not exist in a high enough fraction to guide the properties of the composite with their own interaction properties. In Table 8, we compare the stiffness, strength and toughness values with pure BC (expressed as a ratio with pure BC).

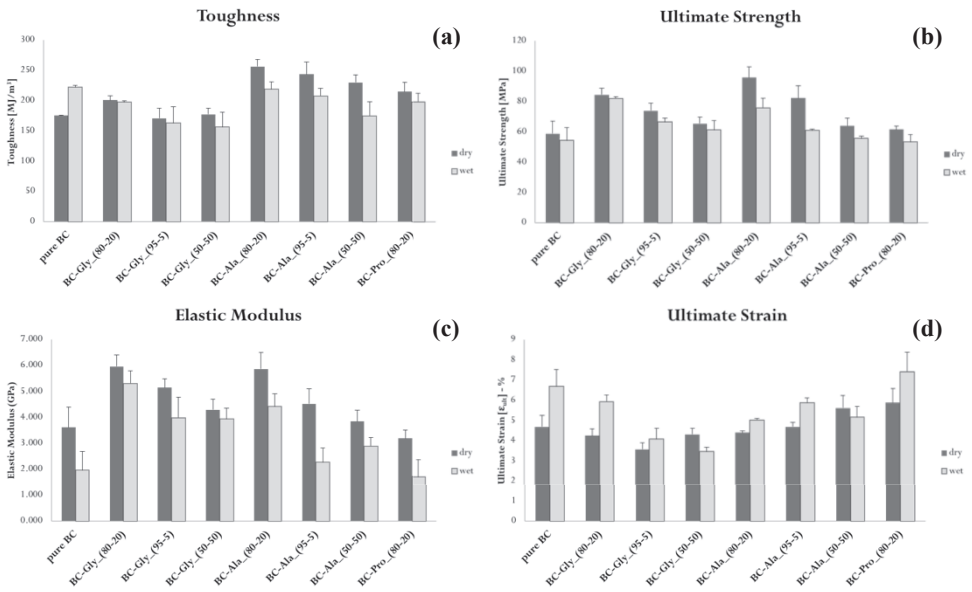

Figure 14 – a) toughness, b) ultimate strength, c) elastic modulus and d) ultimate strain comparison for composite samples

Biomaterials have a variety of applications in the body, requiring distinctive mechanical characteristics for the specific application. Bone for example, requires high stiffness and low elasticity, while wound dressings must be elastic and flexible (Purbrick & Ambrosio, 2010). One of the major problems in manufacture of biomaterials is in the mechanical incompatibility of the biomaterial with the host material. For example, in orthopaedic surgery, a stiffness mismatch between bone and a metallic or ceramic implant may result in difficulties in bone remodelling and healing (Ramakrishna, Mayer, Wintermantel, & Leong, 2001). There are also other factors that should be considered in designing and manufacturing biomaterials, such as pH sensitivity, hydrophobicity or hydrophobicity, surface topology and chemical activity which defines the characteristics of the biomaterials. Therefore, it is important to be able to manipulate the properties of composite biomaterials.

4.3. TEMPO-mediated oxidised bacterial cellulose/amino acid

In the previous sections, we focused on the identification of key amino acids contributing to the adhesive properties of flagelliform silk, and subsequently using the

same relevant amino acids to bind bacterial cellulose. We hypothesised that the high mobility of amino acid might compensate the β-spiral structure of flagelliform silk by providing a flexible and stable hydrogen bonding network. To further investigate our hypothesis, amino acids were immobilised on TEMPO-oxidised BC and the mechanical performance were determined by both modelling and experimentation (Mahdi Pahlevan, Toivakka, & Alam, 2018).

In the TEMPO-oxidation of bacterial cellulose, 2,2,6,6-tetramethylpiperidine-1-oxyl radical (TEMPO) oxidises the C6 primary hydroxyl on the cellulose chains to form C6 carboxylate groups (Yao, et al., 2017). These carboxylic groups allow for the chemical (covalent) functionalisation of BC by bio-active molecules such as amino acids. In this process, we can take advantage of TEMPO oxidized BC to be further modified with various functionalities to the material via carboxylic groups (Saska, et al., 2012) (Li, et al., 2013). It includes hydrophilic, aliphatic and aromatic amino acid groups (Kalaskar, Ulijn, Gough, & , 2010). Primary amino acid groups provide access for further modification such as preparing nanoparticles without any transfection reagents for easy cell uptake (Nikolajski, Wotschadlo, Clement, & Heinze, 2012), strong antimicrobial activity that can be incorporated by attaching silver nanoparticles (AgNPs) (Huang, Chen, Jiang, & Li, 2013) or amino alkyl groups (Fernandes, et al., 2013) to the carboxylate groups. These modifications are applied in variety of medical applications specifically in wound dressing materials (Carolina Andreia Cateto, 2011) (Kalaskar, Ulijn, Gough, & , 2010). The main focus of previous studies on amino acid modified BC was the characterisation of different functionalities resulting from the side chains and less on the mechanical performance of such materials. Herein, we studied the mechanical properties of the manufactured material, which plays a decisive role in its final biomedical or industrial application.

4.3.1. Molecular modelling

The intermolecular and potential energy for each sample was monitored during the process of molecular self-assembly. Molecular dynamics simulations were performed to steady state at the lowest energy of the system, Figure 15. Table 9 shows the lowest intermolecular energy at steady state and the number of hydrogen bonds at steady state. In this table, BC composites with monomeric amino acids retain higher intermolecular energies than equivalent TOBC-AA molecules. Both are nevertheless higher in energy than pure BC. The slightly higher intermolecular energy of TOBC-

AA (specifically TOBC-Ala) compared to pure BC is the result of a small increase in hydrogen bond formation, and a subsequent increase in van der Waals interactions due to extra amino acids on the side chains.

On the contrary, the high stiffness of bacterial cellulose crystalline structures retards any evident changes in the molecular conformation of packed bacterial cellulose molecules. The lack of mobility prevents the formation of a hydrogen bond network that was present in BC-AA, and hence a limited "reach" for self-healing coupled to a limited movement about the fixed ends, leading to lower adhesion in TOBC-AA samples.

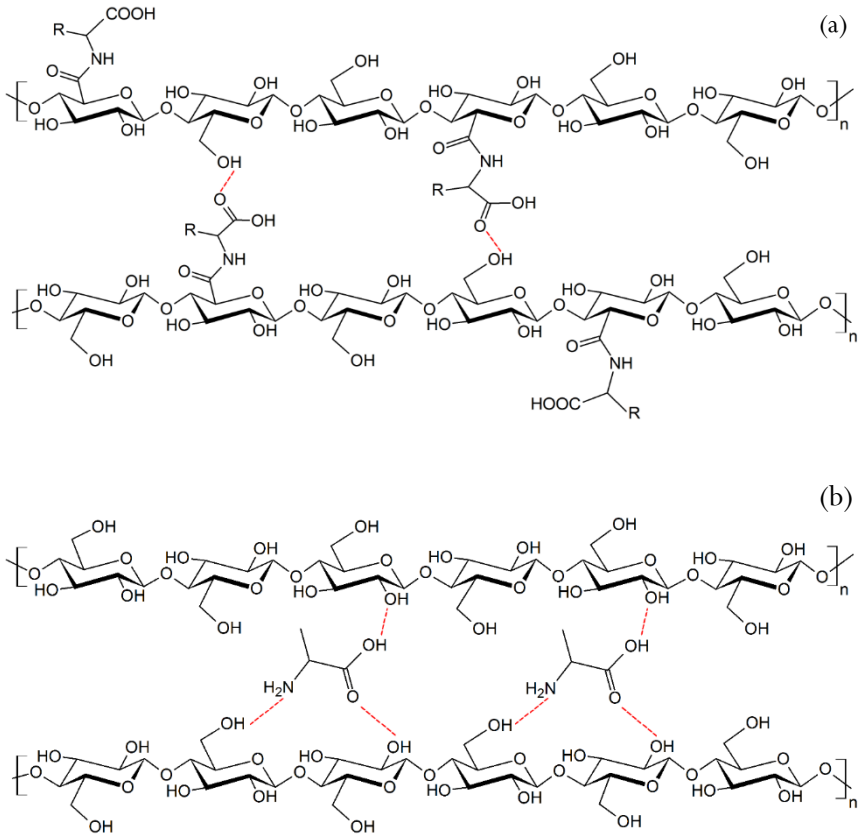

Figure 15 – Schematic illustration of a) TOBC-Ala and b) BC-monomeric Ala after self-assembly. Red hashed lines represent possible hydrogen bond formation sites. Monomeric amino acid in bacterial cellulose has higher potential of forming hydrogen bonds.

Table 9 - Number of hydrogen bonds between molecules in simulated samples and the intermolecular energies for each system after self-assembly. The intermolecular energy is a summation of both the electrostatic and van der Waals interactions. TOBC-Ala, TOBC-Gly and TOBC-Pro values are from the present work and are compared against values for BC, BC-Ala, BC-Gly and BC-Pro (with free moving amino acids) from our previous work (M Pahlevan, Polymer, & 2016, n.d.).

	Intermolecular energy kcal/mol	Maximum number of H-bond
Pure-BC	-218	7
TOBC-Ala	-307	11
TOBC-Gly	-255	10
TOBC-Pro	-245	8
BC-Ala	-357	16
BC-Gly	-348	14
BC-Pro	-324	12

4.3.2. FTIR spectroscopy

Figure 16(a) shows the FTIR ATR transmittance spectra of bacterial cellulose before and after TEMPO-mediated oxidation and amino acid grafting. In BC the main spectral peaks appear at 3340 cm^{-1} for OH stretching, two peaks indicating CH group; peak at 2893 cm^{-1} for CH stretching in CH_2 groups and at 1428 cm^{-1} for CH_2 symmetric bending and peak at 1162 cm^{-1} corresponds to antisymmetric bridge C-O-C stretching which is from glycosidic linkages within cellulose (Barud, et al., 2008). Compared to pure BC, TOBC sodium salt has a clear peak at 1573 cm^{-1}, Figure 16(a), which corresponds to a C=O vibration on a carboxylate group and confirms the successful oxidation of bacterial cellulose (A Morin, C, & 2016, n.d.). The carboxylate group attaches on the C6 position of the glycopyranose ring structure of cellulose.

In

Figure 16(a), the vibrational peak from the NH^{3+} group in amino acid appears in the wavenumber range of 1480 cm^{-1} to 1550 cm^{-1} and following amino acid grafting on the carboxylic group, the peak at 1515 cm^{-1} on non-reacted TOBC is diminished. This peak corresponds with the amine group in the monomeric glycine molecule and

confirms amino acid coupling to oxidised BC. A carboxylic COO^- asymmetric (νas) stretch from the amino acid typically arises between 1540 cm^{-1} and 1680 cm^{-1} (Barth, 2000) (Lydia Caroline, Sankar, Indirani, & Vasudevan, 2009). A strong peak is visible in TOBC with unreacted alanine, TOBC-Ala, TOBC-Gly and TOBC-Pro at 1605 cm^{-1}. H-bond formation usually appears in the range of 1610 cm^{-1} to 1620 cm^{-1} and on the shoulder of the COO^- band (Lydia Caroline, Sankar, Indirani, & Vasudevan, 2009). These peaks can be identified by deconvolution of the spectra within this range.

Figure 16(c), shows the clear peak at 1616 cm^{-1}, which corresponds to H-bond formation in some of the TOBC-AA composites. In this spectrum, the intensity of the TOBC-Ala peak is the highest relative peak, evidencing hydrogen bonding presence in this biomaterial. A smaller relative peak is noted in TOBC-Gly biomaterial and no peak is seen at all in the TOBC-Pro biomaterial. Table 10 summarises noteworthy peaks in these biomaterials.

Table 10 - Summary of relevant FTIR spectral peaks during amino acid modification of TEMPO oxidised bacterial cellulose chemical reaction process.

	Chemical bond	Absorption wavelength
(I)	OH stretching on BC	3340 cm^{-1}
(II)	CH groups on BC	2893 cm^{-1}
(III)	Asymmetric carboxylic COO- stretch on the amino acids	1605 cm^{-1}
(IV)	C=O vibration of carboxylate anion on TOBC-Na	1573 cm^{-1}
(V)	NH^{3+} on amine group present with unreacted amino acid and disappears after grafting to TOBC	1515 cm^{-1}
(VI)	CH_2 group on BC	1428 cm^{-1}
(VII)	Anti-symmetric bridge C-O-C stretching	1162 cm^{-1}
(VIII)	Hydrogen bond formation on TOBC-AA	1616 cm^{-1}

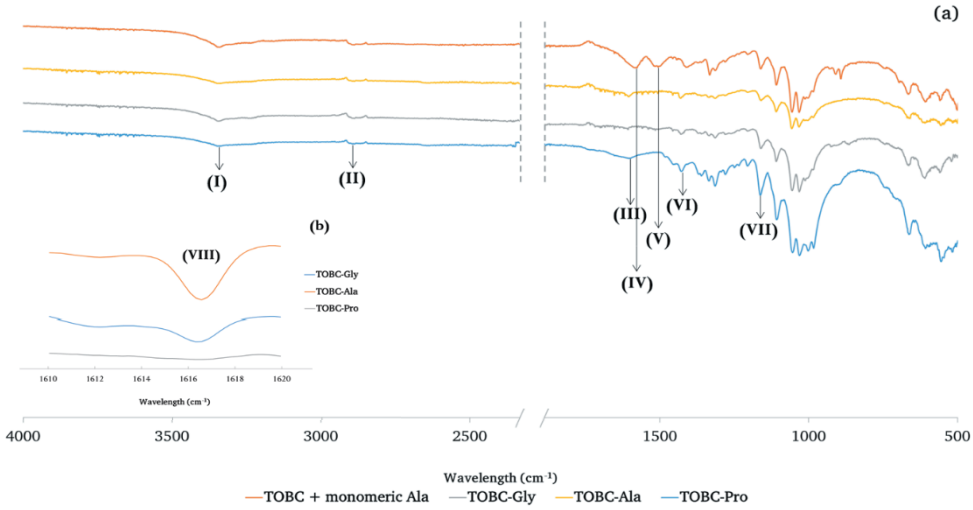

Figure 16 - FTIR spectra for (a) bacterial cellulose peaks present in BC based composite samples; non-reacted TOBC with monomeric alanine, TOBC-Gly, TOBC-Ala and TOBC-Pro, and (b) H-bond peaks for TOBC-AA after spectral deconvolution.

4.3.3. Experimental mechanical tests

Tensile testing was performed on our samples and initial results exhibit no improvement in the toughness of manufactured TOBC-AA samples over pure BC, Figure 16(a). These samples have slightly higher elastic moduli and ultimate strengths; however, their lower elasticity values make up for this, resulting in a similar overall toughness to that of pure BC, Figure 16 (b), (c) and (d).

The mechanical strength of TOBC-AA samples is higher than that of pure BC. This is related to the initial hydrogen bonding and physical obstruction by amino acid side chains. However, the structure weakens once the initial resistance is broken. The TOBC-AA crystalline molecular structure lacks enough flexibility to provide effective intermolecular interactions, and the lower hydrogen bonding potential results in a relatively similar ultimate strength of TOBC-AA samples to pure BC.

Our modelled molecular structure suggests that the side chains of TOBC-AA are utilized to increase van der Waals interaction and potential hydrogen bond formation. Subjecting the molecules to shear, side chains will interlock and entangle that in turn will increase the intermolecular resistance to shear, which gives rise to elastic modulus of synthesised TOBC-AA samples, Figure 17(c). Alanine and glycine have similar structures and form hydrogen bonds, but the extra methyl group on alanine increases collisions and consequently higher van der Waals interactions. Proline, on the other hand, has a large ring that prevents the effective formation of hydrogen bonds. Therefore, TOBC-Pro does not reach the same levels of strength as TOBC-Ala.

Here, the amino acid side chains connect to water molecules via electrostatic attraction, therefore unlike pure BC, the toughness of TOBC-AA samples will decrease when wet. The elastic modulus of wet samples exhibits opposing trends to dry samples, and TOBC-Pro is noted to have a higher E-modulus compared to TOBC-Gly and TOBC-Ala. Here, water molecules compete over potential hydrogen bonding sites with the amino acid molecules, which reduces biomolecular interactions and weakens the biomaterials. Furthermore, the large ring on the molecule of proline effectively blocks incoming water, which results in an elevated elastic modulus in TOBC-Pro samples as compared to TOBC-Ala and TOBC-Gly. The mechanical properties of all dry and wet samples are compared in Figure 17 and stress-strain curves of representative manufactured samples are depicted in Figure 18.

Monomeric alanine and glycine exhibit higher strength, stiffness and toughness as compared to TOBC-AA biomaterials, Table 11. The higher mobility of monomeric amino acid results in the easier formation of intermolecular hydrogen bonds, and promotes the self-healing mechanism, which in turn increases the elasticity of BC-AA. Proline is the exception of the three monomeric free-moving amino acids since it has a large ring structure that acts as an obstruction to H-bond formation. BC-Ala offers up to 40% higher toughness and ultimate strength and a considerably higher elastic modulus as compared to pure BC.

Other factors can also be considered in determining the mechanical performance of TOBC-AA such as the modification of pH, which can be further investigated in the future study.

Table 11 - Dry density, specific stiffness, specific strength and mechanical properties normalised by BC values for bacterial cellulose with amino acids and amino acid modified TEMPO oxidised bacterial cellulose and pure BC as reference. RH95 - relative humidity at 95°C. The values for BC-Ala, BC-Pro and BC.

	(ρ) - g/cm³	E/ρ - MNm/Kg	σ_{ult}/ρ - kNm/Kg	E/E(BC) %	G/G(BC) %	σ/σ(BC) %
pure BC	0.969	3.7	60.6	1.0	1.0	1.0
pure BC_RH95		2.0	56.2	0.5	1.3	0.9
BC-Gly	0.834	7.1	101.1	1.7	1.1	1.4
BC-Gly_RH95		6.4	98.5	1.5	1.1	1.4
BC-Ala	0.862	6.8	111.0	1.6	1.5	1.6
BC-Ala_RH95		5.1	87.9	1.2	1.2	1.3
BC-Pro	1.026	3.1	60.0	0.9	1.2	1.0
BC-Pro_RH95		1.7	52.0	0.5	1.1	0.9
TOBC-Gly	0.915	4.5	66.1	1.2	1.0	1.1
TOBC-Gly_RH95		3.3	52.2	0.9	0.7	0.9
TOBC-Ala	0.932	4.5	72.2	1.2	1.0	1.2
TOBC-Ala_RH95		2.5	51.0	0.7	0.9	0.8
TOBC-Pro	0.988	3.6	56.9	1.0	1.0	1.0
TOBC-Pro_RH95		3.2	50.8	0.9	0.8	0.9

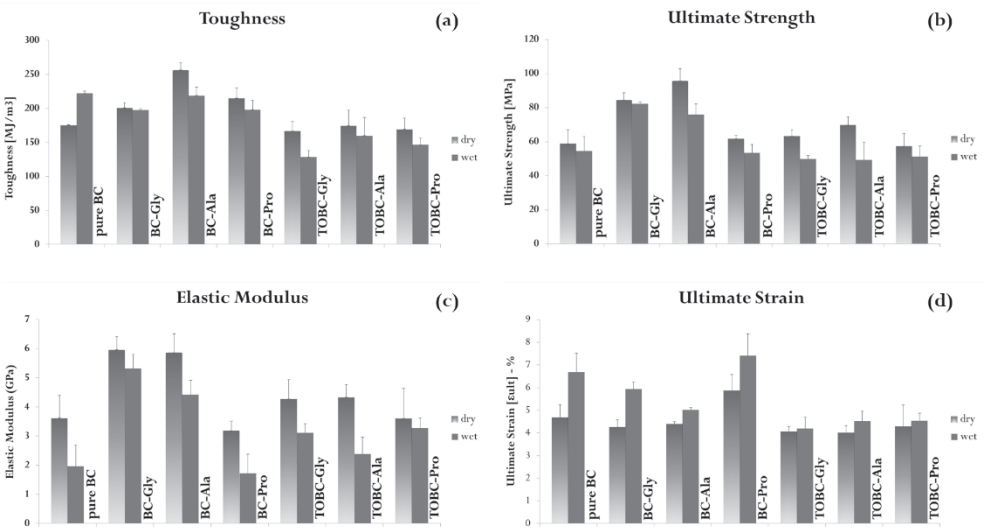

Figure 17 - Histograms showing a) ultimate strength, b) toughness, c) elastic modulus and d) ultimate strain comparison for pure BC, TOBC-AA and BC- monomeric amino acid in both dry and wet states. Error bars indicate the standard deviation from an arithmetic mean.

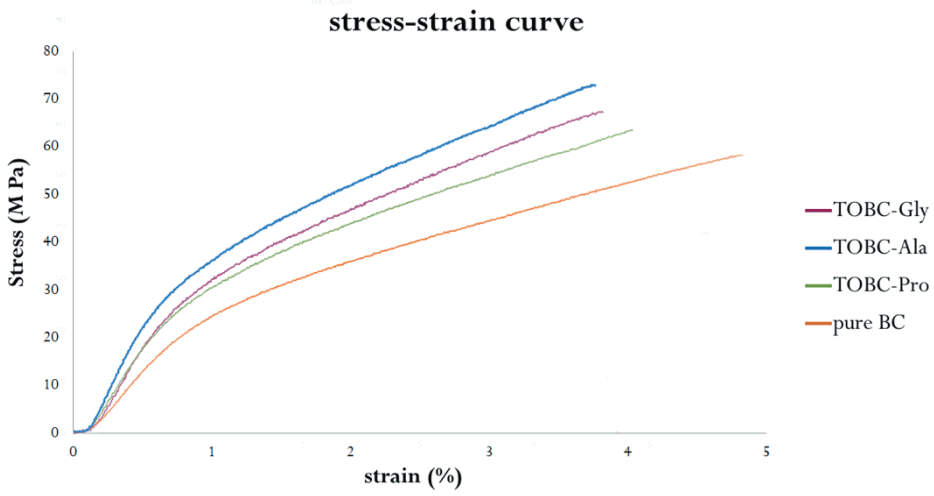

Figure 18 – Stress-strain curve for three samples for the TOBC-Gly, TOBC-Ala and TOBC-Pro samples and pure BC as reference

5. Concluding remarks and outlook

5.1. Conclusion

In this thesis, we initially focused on understanding the mechanical properties of two major silk proteins from spiders, dragline and flagelliform silk. We then took inspiration from the functionalities of their molecular primary and secondary structures in order to produce composite biomaterials with different mechanical properties.

Based on earlier studies, we hypothesised that electrostatic charges enforce a certain deformation mechanism in dragline silk, which better dissipates the impact energy of captured prey. Molecular dynamics simulations were employed to model MaSp1 deformation from a folded state and under the influence of electrostatic pulling forces. The following conclusions can be made:

The 'concertina-like' mechanisms of deformation yield higher strains to failure when there are a greater number of amorphous segments along the protein molecules.

A 'second catch' mechanism was present which recreates β-sheets via hydrogen bonding, then giving rise to a very high level of localised toughness (strength and stretch coupled).

Localised molecular-level 'toughening' of spider silk results solely from electrostatic forces as evidenced and permits the web to absorb large levels of impaction energy just before the insect makes contact.

Consequently, a combination of highly crystalline bacterial cellulose and elastic flagelliform silk was chosen to design a composite material that mimics the mechanical characteristics of MaSp1 with. Additional modelling of this material was undertaken to discern the potential manufacturing routes for mimicking certain desired effects.

Initial simulations revealed flagelliform silk sequences and free predominant amino acids from flagelliform silk (proline, alanine and glycine) yield similar mechanical properties when combined with BC

The higher mobility of monomeric amino acids and H-bond formation (hence self-healing) improves the adhesion between BC molecules as compared to flagelliform silk molecules

Alanine and glycine bioglues are superior to proline and have specific strength values exceeding those for spider dragline silk and bone, and specific stiffness values exceeding that of collagen

Additionally, we validated BC-AA system against similar systems with reduced degrees of freedom (TEMPO/grafted) by both modelling and experimentation.

Modelling and experimental results confirm that the absence of flexible amorphous regions in TOBC-AA systems reduce the overall toughness of the composite as compared to BC-Flag and BC-AA systems.

Crystalline rigid materials lack sufficient mobility to form stable H-bonding networks and are unable to reach a desired structural conformation suitable for mechanical enhancement.

5.2. Future work

There are two approaches in this project that can be the case for future studies; computational and experimental. The computational aspect is based on MD simulation of MaSp1 and flagelliform silk and bacterial cellulose in the composite with silk materials. The study can be extended by subjecting the model structures to strain, pull out or peel stress after self-assembly of the system. The simulations will provide us with a more detailed and accurate understanding of the molecular behaviour of these materials under stress.

Recent advances in production of recombinant silk can be a potential outlook for further experimental work using combined recombinant MaSp1 and flagelliform silks. Further investigations could then be conducted into the adhesive properties of these silks as a composite with bacterial cellulose.

6. Bibliography

Agnarsson, I., Kuntner, M., & Blackledge, T. (2010). Bioprospecting Finds the Toughest Biological Material: Extraordinary Silk from a Giant Riverine Orb Spider. *PLoS ONE, 5*.

Agnarsson, I., Kuntner, M., & Blackledge, T. A. (2010). Bioprospecting Finds the Toughest Biological Material: Extraordinary Silk from a Giant Riverine Orb Spider. *PLoS ONE, 5*(9).

Altman, G. H., Diaz, F., Jakuba, C., Calabro, T., Horan, R. L., Chen, J., . . . Kaplan, D. L. (2003). Silk-based biomaterials. *Biomaterials, 24*, 401–416.

An, B., Hinman, M. B., Holland, G. P., Yarger, J. L., & Lewis, R. V. (2011). Inducing β-Sheets Formation in Synthetic Spider Silk Fibers by Aqueous Post-Spin Stretching. *Biomacromolecules, 12*, 2375–2381.

An, B., Tang-Schomer, M., Huang, W., He, J., Jones, J., Lewis, R., & Kaplan, D. (2015). Physical and biological regulation of neuron regenerative growth and network formation on recombinant dragline silks. *Biomaterials, 48*, 137–146.

An, B., Tang-Schomer, M., Huang, W., He, J., Jones, J., Lewis, R., & Kaplan, D. (2015). Physical and biological regulation of neuron regenerative growth and network formation on recombinant dragline silks. *Biomaterials, 48*, 137-146.

Armougom, F., Moretti, S., Keduas, V., & Notredame, C. (2006). The iRMSD: a local measure of sequence alignment accuracy using structural information. *Bioinformatics, 22*, 35-39.

Asakura, T., Okonogi, M., Nakazawa, Y., & Yamauchi, K. (2006). Structural Analysis of Alanine Tripeptide with Antiparallel and Parallel beta-Sheet Structures in Relation to the Analysis of Mixed beta-Sheet Structures in Samia cynthia ricini Silk Protein Fiber Using Solid-State NMR Spectroscopy. *Journal of American Chemical Society, 128*, 6231-6238.

Ayoub, N. A., Garb, J. E., Tinghitella, R. M., Collin, M. A., & Hayashi, C. Y. (2007). Blueprint for a High-Performance Biomaterial: Full-Length Spider Dragline Silk Genes. *PLoS ONE*(6), 1-13.

Baoyong, L., Jian, Z., Denglong, C., & Min, L. (2010). Evaluation of a new type of wound dressing made from recombinant spider silk protein using rat models. *Burns, 36*, 891-896.

Barth, A. (2000). The infrared absorption of amino acid side chains. *Progress in Biophysics & Molecular Biology, 74*, 141-173.

Barud, H., Assunção, R., Martines, M., Marques, R., Messaddeq, Y., & Ribeiro, S. (2008). Bacterial cellulose–silica organic–inorganic hybrids. *Journal of Sol-Gel Science and Technology, 46*, 363-367.

Bosia, F., Buehler, M. J., & Pugno, N. M. (2010). Hierarchical simulations for the design of supertough nanofibers inspired by spider silk. *Physical Review, 82*.

Bratzel, G., & Buehler, M. J. (2011). Molecular Mechanics of Silk Nanostructures Under Varied Mechanical Loading. *Biopolymers, 97*, 408-417.

Bratzel, G., & Buehler, M. J. (2012). Sequence-structure correlations in silk: Poly-Ala repeat of N. clavipes MaSp1 is naturally optimized at a critical length scale. *Journal of the Mechanical Behavior of Biomedical Materials, 7*, 30-40.

Brooks, C. L. (2002). Protein and Peptide Folding Explored with Molecular Simulations. *Accounts of Chemical Research, 35*, 447-454.

Buehler, M. J. (2010). Tu(r)ning weakness to strength. *Nano Today, 5*, 379—383.

Buehler, M. J., & Yung, Y. (2009). Deformation and failure of protein materials in physiologically extreme conditions and disease. *Nature Materials, 8*, 175-188.

Buehler, M. J., Keten, S., & Ackbarow, T. (2008). Theoretical and computational hierarchical nanomechanics of protein materials: Deformation and fracture. *Progress in Materials Science, 53*, 1101–1241.

Caflisch, A., & Paci, E. (2005). Molecular Dynamics Simulations to Study Protein Folding and Unfolding. In J. B. Kiefhaber (Ed.), *Protein Folding Handbook* (pp. 1143–1169).

Cai, Z., & Kim, J. (2009). Bacterial cellulose/poly(ethylene glycol) composite: characterization and first evaluation of biocompatibility. *Cellulose, 16*, 1033-1045.

Carolina Andreia Cateto, A. R. (2011). Amino acid modified cellulose whiskers. *RSC Advances, 1*, 1695-1697.

Cathy J. Ridgway, J. S. (2011). Competitive Absorption of Polar and Non-Polar Liquids into Latex Bound Porous Structures of Fine Ground Calcium Carbonate. *Transport in Porous Media, 86*, 945–964.

Cetinkaya, M., Xiao, S., & Gräter, F. (2011). Bottom-up computational modeling of semi-crystalline fibers: from atomistic to continuum scale. *Physical Chemistry Chemical Physics, 13*, 10426-10429.

Cetinkaya, M., Xiao, S., & Gräter, F. (2011). Effects of crystalline subunit size on silk fiber mechanics. *Soft Matter, 7*, 8142-8148.

Chen, X., Shao, Z., & Vollrath, F. (2006). The spinning processes for spider silk. *Soft Matter, 2*, 448–451.

Cornell, W. D., Cieplak, P., Bayly, C. I., Gould, I. R., Merz, K. M., Ferguson, D. M., . . . Kollman, P. A. (1995). A Second Generation Force Field for the Simulation of Proteins, Nucleic Acids, and Organic Molecules. *Journal of American Chemical Society, 117*, 5179-5197.

Craig, C. L., Hsu, M., Kaplan, D., & Piercea, N. E. (1999). A comparison of the composition of silk proteins produced by spiders and insects. *International Journal of Biological Macromolecules, 24*, 109–118.

Cranford, S. W., & Buehler, M. J. (2012). *Biomateriomics* (1st ed.). Springer.

Cranford, S., & Buehler, M. J. (2010). Materiomics: biological protein materials, from nano to macro. *Nanotechnology, Science and Applications, 3*, 127-148.

Czaja, W. K., Young, D. J., Kawecki, M., & Brown, R. (2007). The Future Prospects of Microbial Cellulose in Biomedical Applications. *Biomacromolecules, 8*, 1–12.

da Silva, R., Maria R., S., Helen P., B., Sônia F., Z., Cleverton L., P., Lucy, O., & Rilton A., d. F. (2016). Hydrophilicity improvement of mercerized bacterial cellulose films by polyethylene glycol graft. *International Journal of Biological Macromolecules, 86*, 599-605.

Dammstrom, S., Salmen, L., & Gatenholm, P. (2005). The effect of moisture on the dynamical mechanical properties of bacterial cellulose/glucuronoxylan nanocomposites. *Polymer*, 10364–10371.

Eisoldt, L., Smith, A., & Scheibel, T. (2011). Decoding the secrets of spider silk. *Materials Today, 14*, 80-86.

Fernandes, S. C., Patrizia, S., Ana, A.-V., Teodoro, P., Arantxa, E., Armando, J. S., . . . Carmen, S. F. (2013). Bioinspired Antimicrobial and Biocompatible Bacterial Cellulose Membranes Obtained by Surface Functionalization with Aminoalkyl Groups. *ACS Applied Materials & Interfaces, 5*, 3290-3297.

Foreman, J. P., Porter, D., Behzadi, S., & Jones, F. R. (2008). A model for the prediction of structure–property relations in cross-linked polymers. *Polymer, 49*, 5588–5595.

Foreman, J. P., Porter, D., Behzadi, S., & Jones, F. R. (2008). A model for the prediction of structure–property relations in cross-linked polymers. *Polymer, 49*, 5588–5595.

Fu, C., Porter, D., Chen, X., Volrath, F., & Shao, Z. (2011). Understanding the Mechanical Properties of Antheraea Pernyi Silk—From Primary Structure to Condensed Structure of the Protein. *Advanced Functional Materials, 21*, 729–737.

Fu, C., Shao, Z., & Vollrath, F. (2009). Animal silks: their structures, properties and artificial production. *Chemical Communications, 43*, 6515–6529.

George, J., Ramana, V. K., Sabapathy, N. S., Jagannath, H. J., & Bawa, S. A. (2005). Characterization of chemically treated bacterial (Acetobacter xylinum) biopolymer: Some thermo-mechanical properties. *International Journal of Biological Macromolecules, 37*, 189–194.

Goelzer, F., Faria-Tischer, P., Vitorino, J., Sierakowski, M. R., & Tischer, C. (2009). Production and characterization of nanospheres of bacterial cellulose from Acetobacter xylinum from processed rice bark. *Materials Science and Engineering C, 29*, 546–551.

Gosline, J., DeMont, E., & Denny, M. (1986). The structure and properties of spider silk. *Endeavour, 10*, 37-43.

Grande, C. j., Torres, F. G., Gomez, C. M., & Bano, C. (2009). Nanocomposites of bacterial cellulose/hydroxyapatite for biomedical applications. *Acta Biomaterialia, 5*, 1605–1615.

Granovsky, A. A. (n.d.). Retrieved from Firefly version 8: www http://classic.chem.msu.su/gran/firefly/index.html

Grant, J., Pickup, B., Sykes, M., Kitchen, C., & Nicholls, A. (2007). A simple formula for dielectric polarisation energies: The Sheffield Solvation Model. *Chemical Physics Letters, 441*, 163-166.

Greving, I., Cai, M., Vollrath, F., & Schniepp, H. C. (2012). Shear-Induced Self-Assembly of Native Silk Proteins into Fibrils Studied by Atomic Force Microscopy. *Biomacromolecules, 13*, 676–682.

Grunwald, I., Rischka, K., Kast, S. M., Scheibel, T., & Bargel, H. (2009). Mimicking biopolymers on a molecular scale nano(bio)technology based on engineered proteins. *The Royal Society, 367*, 1727-1747.

Hakimi, O., Knight, D. P., Vollrath, F., & Vadgama, P. (2007). Spider and mulberry silkworm silks as compatible biomaterials. *Composites, 38*, 324–337.

Hardy, J. G., & Scheibel, T. (2010). Composite materials based on silk proteins. *Progress in Polymer Science, 35*, 1093–1115.

Hardy, J. G., & Scheibel, T. R. (2009). Silk-inspired polymers and proteins. *Bionanotechnology II: from Biomolecular Assembly to Applications, 37*, 677–681.

Hardy, J. G., Leal-Egana, A., & Scheibel, T. R. (2013). Engineered Spider Silk Protein-Based Composites for Drug Delivery. *Macromolecular Bioscience, 13*, 1431–1437.

Hardy, J. G., Römer, L. M., & Scheibel, T. R. (2008). Polymeric materials based on silk proteins. *Polymer, 49*, 4309–4327.

Harmer, A. M., Blackledge, T. A., Madin, J. S., & Herberstein, M. E. (2011). High-performance spider webs: integrating biomechanics, ecology and behaviour. *Journal of Royal Society Interface, 8*, 457-471.

Harris, T. I., Gaztambide, D. A., Day, B. A., Brock, C. L., Ruben, A. L., Jones, J. A., & Lewis, R. V. (2016). Sticky Situation: An Investigation of Robust Aqueous-Based Recombinant Spider Silk Protein Coatings and Adhesives. *Biomacromolecules, 17*, 3761-3772.

Hartmann, S., & Wunderle, B. (2012). Pull-Out Testing of SWCNTs Simulated by Molecular Dynamics. *International Journal of Theoretical and Applied Nanotechnology, 1*, 59-65.

Hayashi, C. Y., & Lewis, R. V. (1998). Evidence from Flagelliform Silk cDNA for the Structural Basis of Elasticity and Modular Nature of Spider Silks. *J. Mol. Biol., 275*, 773-784.

Hayashi, C. Y., & Lewis, R. V. (2001). Spider flagelliform silk: lessons in protein design, gene structure, and molecular evolution. *BioEssays, 23*, 750-756.

Heim, M., Ackerschott, C. B., & Scheibel, T. (2010). Characterization of recombinantly produced spider flagelliform silk domains. *Journal of Structural Biology, 170*, 420-425.

Heim, M., Römer, L., & Scheibel, T. (2009). Hierarchical structures made of proteins. The complex architecture of spider webs and their constituent silk proteins. *Chemical Society Reviews, 39*, 156–164.

Hijirida, D., Do, K., Michal, C., Wong, S., Zax, D., & Jelinski, L. (1996). 13C NMR of Nephila clavipes major ampullate silk gland. *Biophysical Journal, 71*, 3442–3447.

Hofer, M., Winter, G., & Myschik, J. (2012). Recombinant spider silk particles for controlled delivery of protein drugs. *Biomaterials, 33*, 1554–1562.

Holland, G. P., Lewis, R. V., & Yarger, J. L. (2004). WISE NMR Characterization of Nanoscale Heterogeneity and Mobility in Supercontracted Nephila clavipes Spider Dragline Silk. *Journal of American Chemical Society, 126*, 5867-5872.

Hsieh, Y., Yano, H., Nogi, M., & Eichhorn, S. (2008). An estimation of the Young's modulus of bacterial cellulose filaments. *Cellulose August 2008, Volume 15, Issue 4, pp 507–513, 15*(4), 507-513.

Hu, X., Vasanthavada, K., Kohler, K., McNary, S., Moore, A., & Vierra, C. (2006). Molecular mechanisms of spider silk. *Cellular and Molecular Life Sciences, 63*, 1986–1999.

Hu, Y., & Catchmark, J. M. (2011). In vitro biodegradability and mechanical properties of bioabsorbable bacterial cellulose incorporating cellulases. *Acta Biomaterialia, 7*, 2835–2845.

Huang, M., Chen, F., Jiang, Z., & Li, Y. (2013). Preparation of TEMPO-oxidized cellulose/amino acid/nanosilverbiocomposite film and its antibacterial activity. *International Journal of Biological Macromolecules, 62*, 608-613.

Hull, D., & Clyne, T. (1996). *An Introduction to Composite Materials* (2 ed.). Cambridge University Press.

Humenik, M., Smith, A. M., & Scheibel, T. (2011). Recombinant Spider Silks—Biopolymers with Potential for Future Applications. *Polymers, 3*, 640-661.

Humphrey, W., Dalke, A., & Schulten, K. (1996). VMD - Visual Molecular Dynamics. *Journal of Molecular Graphics, 14*, 33-38.

Iguchi, M., Yamanaka, S., & Budhiono, A. (2000). Bacterial cellulose—a masterpiece of nature's arts. *Journal of Materials Science, 35*(2), 261-270.

Isogai, A., Saito, T., & Fukuzumi, H. (2011). TEMPO-oxidized cellulose nanofibers. *Nanoscale, 3*, 71-85.

Jansson, R., Thatikonda, N., Lindberg, D., Rising, A., Johansson, J., Nygren, P.-Å., & Hedhammar, M. (2014). Recombinant Spider Silk Genetically Functionalized with Affinity Domains. *Biomacromolecules, 15*, 1696−1706.

Jenkins, J. E., Creager, M. S., Lewis, R. V., Holland, G. P., & Yarger, J. L. (2010). Quantitative Correlation between the Protein Primary Sequences and Secondary Structures in Spider Dragline Silks. *Biomacromolecules, 11*, 192-200.

Jones, J., Harris, T., Tucker, C., Berg, K., Christy, S., Day, B., & Lewis, R. (2015). More Than Just Fibers: An Aqueous Method for the Production of Innovative Recombinant Spider Silk Protein Materials. *Biomacromolecules, 16*, 1418-1425.

Jones, J., Harris, T., Tucker, C., Berg, K., Christy, S., Day, B., . . . Lewis, R. (2015). More Than Just Fibers: An Aqueous Method for the Production of Innovative Recombinant Spider Silk Protein Materials. *Biomacromolecules, 16*, 1418−1425.

Kalaskar, D., Ulijn, R., Gough, J., & . (2010). Characterisation of amino acid modified cellulose surfaces using ToF-SIMS and XPS. *Cellulose, 17*, 747-756.

Keten, S., & Buehler, M. J. (2008). Asymptotic Strength Limit of Hydrogen-Bond Assemblies in Proteins at Vanishing Pulling Rates. *Physical Review Letters, 100*.

Keten, S., & Buehler, M. J. (2010b). Nanostructure and molecular mechanics of spider dragline silk protein assemblies. *Journal of the Royal Society Interface, 7*, 1709−1721.

Keten, S., & Buehler, M. J. (2010c). Atomistic model of the spider silk nanostructure. *Applied Physics Letters, 96*, 153701.

Keten, S., Xu, Z., Britni, I., & Markus, B. J. (2010a). Nanoconfinement controls stiffness, strength and mechanical toughness of beta-sheet crystals in silk. *Nature Materials, 9*, 359-367.

Krishnaji, S. T., Bratzel, G., Kinahan, M., Kluge, J., Staii, C., Wong, J., . . . Kaplan, D. (2013). Sequence–Structure–Property Relationships of Recombinant Spider Silk Proteins: Integration of Biopolymer Design, Processing, and Modeling. *Adv. Funct. Mater., 23*, 241-253.

Krishnaji, S., Huang, W., Cebe, P., & Kaplan, D. (2014). Infl uence of Solution Parameters on Phase Diagram of Recombinant Spider Silk-Like Block

Copolymers. *Macromol. Chem. Phys., 215*, 1230–1238.

Lammel, A., Schwab, M., Hofer, M., Winter, G., & Scheibel, T. (2011). Recombinant spider silk particles as drug delivery vehicles. *Biomaterials, 32*, 2233-2240.

Lammel, A., Schwab, M., Hofer, M., Winter, G., & Scheibel, T. (2011). Recombinant spider silk particles as drug delivery vehicles. *Biomaterials, 32*, 2233-2240.

Leal-Egaña, A., & Scheibel, T. (2010). Silk-based materials for biomedical applications. *Biotechnology Applied Biochemistry, 55*, 155-167.

Lewicka, M., Hermanson, O., & Rising, A. U. (2012). Recombinant spider silk matrices for neural stem cell cultures. *Biomaterials, 33*, 7712-7717.

Lewis, R. V. (2003). Sequences, Structures, and Properties of Spider Silks. In P. R. Shewry, A. S. Tatham, & A. J. Bailey (Eds.), *Elastomeric Proteins, Structures, Biomechanical Properties, and Biological Roles.* Cambridge University Press.

Li, L., Shuai, Z., Jin, Z., Zhen, X. Z., Hongqi, H., Zhenxiang, X., & Jin, K. K. (2013). TEMPO-mediated oxidation of microcrystalline cellulose: Influence of temperature and oxidation procedure on yields of water-soluble products and crystal structures of water-insoluble residues. *Fibers and Polymers, 14*, 352-357.

Lin, S., Ryu, S., Tokareva, O., Gronau, G., Jacobsen, M., Huang, W., . . . Buehler, M. (2015). Predictive modelling-based design and experiments for synthesis and spinning of bioinspired silk fibres. *Nature Communications, 6*, 1-12.

Liu, Y., Sponner, A., Porter, D., & Vollrath, F. (2008). Proline and Processing of Spider Silks. *Biomacromolecules, 9*, 116-121.

Lombardi, S. J., & Kaplan, D. L. (1990). The amino acid composition of major ampullate gland silk. {dragline) of Nephila clavipes (Araneae, Tetragnathidae). *The Journal of Arachnology, 18*, 297-306.

Lombardi, S., & Kaplan, D. (1990). The Amino Acid Composition of Major Ampullate Gland Silk (Dragline) of Nephila Clavipes (Araneae, Tetragnathidae). *The Journal of Arachnology, 18*, 297-306.

Luo, H., Guangyao, X., Da, H., Kaijing, R., Fanglian, Y., Yong, Z., . . . Yizao, W. (2013). Characterization of TEMPO-oxidized bacterial cellulose scaffolds for tissue engineering applications. *Materials Chemistry and Physics, 143*, 373-379.

Luo, H., Xiong, G., Hu, D., Ren, K., Yao, F., Zhu, Y., . . . Wan, Y. (2013). Characterization of TEMPO-oxidized bacterial cellulose scaffolds for tissue engineering applications. *Materials Chemistry and Physics, 143*, 373–379.

Lydia Caroline, M., Sankar, R., Indirani, R., & Vasudevan, S. (2009). Growth, optical, thermal and dielectric studies of an amino acid organic. *Materials Chemistry and Physics, 114*, 490-494.

Møller, C., & Plesset, M. (1934). Note on an Approximation Treatment for Many-Electron Systems. *Physical Review, 46*, 618.

Marsano, E. C. (2007). Fibers based on cellulose–silk fibroin blend. *J. Appl. Polym. Sci., 104*, 2187–2196.

Mendes, P. N., Rahal, S. C., Câmara, O., Pereira-Junior, M., Fabris, V. E., Lenharo, S. L., . . . da Cruz Landim-Alvarenga, F. (2009). In vivo and in vitro evaluation of

an Acetobacter xylinum synthesized microbial cellulose membrane intended for guided tissue repair. *Acta Veterinaria Scandinavica 2009, 51:12, 51*.

Morin, A., & Alam, P. (2016). Comparing the properties of Bombyx mori silk cocoons against sericin-fibroin regummed biocomposite sheets. *Materials Science and Engineering: C, 65*, 215-220.

Morin, A., Pahlevan, M., & Alam, P. (2017). Chapter 8: Silk Biocomposites: Structure and Chemistry. In V. Thakur, *Handbook of Composites from Renewable Materials* (pp. 189-205). John Wiley and Sons.

Nikolajski, M., Wotschadlo, J., Clement, J. H., & Heinze, T. (2012). Amino-Functionalized Cellulose Nanoparticles: Preparation, Characterization, and Interactions with Living Cells. *Macromolecular Bioscience, 12*, 920-925.

Nova, A., Keten, S., Pugno, N. M., Redaelli, A., & Buehler, M. J. (2010). Molecular and Nanostructural Mechanisms of Deformation, Strength and Toughness of Spider Silk Fibrils. *Nano Letters, 10*, 2626–2634.

Ohgo, K., Kawase, T., Ashida, J., & Asakura, T. (2006). Solid-State NMR Analysis of a Peptide (Gly-Pro-Gly-Gly-Ala)6-Gly Derived from a Flagelliform Silk Sequence of Nephila clavipes. *Biomacromolecules, 7*, 1210-1214.

Ortega-Jimenez, V., & Dudley, R. (2013). Spiderweb deformation induced by electrostatically charged insects. *Scientific Reports, 3*, 1-4. doi:10.1038/srep02108

Pahlevan, M., & Alam, P. (2016). Flagelliform silk inspired free amino acid bio-glues in bacterial cellulose biomaterials. *Polymer, 97*, 122-130.

Pahlevan, M., Toivakka, M., & Alam, P. (2014). Electrostatic charges instigate 'concertina-like' mechanisms ofmolecular toughening in MaSp1 (spider silk) proteins. *Materials Science and Engineering C, 41*, 329-334.

Pahlevan, M., Toivakka, M., & Alam, P. (2018). Mechanical properties of TEMPO-oxidised bacterial cellulose-amino acid biomaterials. *European Polymer Journal*.

Petersen, N., & Gatenholm, P. (2011). Bacterial cellulose-based materials and medical devices: current state and perspectives. *Applied Microbiology and Biotechnology, 91*, 1277–1286.

Porter, D., & Volrath, F. (2009). Silk as a Biomimetic Ideal for Structural Polymers. *Advanced Materials, 21*, 487–492.

Porter, D., Volrath, F., & Shao, Z. (2005). Predicting the mechanical properties of spider silk as a model nanostructured polymer. *The European Physical Journal E, 16*, 199-206.

Purbrick, M., & Ambrosio, L. (2010). Natural composites: structure–property relationships in bone, cartilage, ligament and tendons. In L. Ambrosio, *Biomedical composites* (pp. 3-24). CRC Press.

Qin, Z., Compton, B., Lewis, J., & Buehler, M. (2015). Structural optimization of 3D-printed synthetic spider webs for high strength. *Nature Communications, 6*.

Quiroz-Castañeda, R. E., & Folch-Mallol, J. L. (2013). Hydrolysis of Biomass Mediated by Cellulases for the Production of Sugars. In A. K. Chandel, *Sustainable Degradation of Lignocellulosic Biomass - Techniques, Applications and Commercialization.* InTech. doi:10.5772/53719

Römer, L., & Scheibel, T. (2008). The elaborate structure of spider silk: Structure and

function of a natural high performance fiber. *Prion, 2*, 154-161.

Ramakrishna, S., Mayer, J., Wintermantel, E., & Leong, K. W. (2001). Biomedical applications of polymer-composite materials: a review. *Composites Science and Technology, 61*, 1189–1224.

Reva, I., Stepanian, S., Plokhotnichenko, A., Radchenko, E., Sheina, G., & Blagoi, Y. (1994). Infrared matrix isolation studies of amino acids. Molecular structure of proline. *Journal of Molecular Structure, 318*, 1-13.

Riekel, C., & Volrath, F. (2001). Spider silk fibre extrusion: combined wide- and small-angle X-ray microdiffraction experiments. *International Journal of Biological Macromolecules, 29*, 203–210.

Rising, A. (2014). Controlled assembly: A prerequisite for the use of recombinant spider silk in regenerative medicine? *Acta Biomaterialia 10 (2014) 1627–1631, 10*, 1627-1631.

Rising, A., Widhe, M., Johansson, J., & Hedhammar, M. (2011). Spider silk proteins: recent advances in recombinant production, structure–function relationships and biomedical applications. *Cell. Mol. Life Sci., 68*, 169-184.

Sai, H., Rui, F., Li, X., Junhui, X., Zhenyou, L., Fei, L., & Ting, Z. (2015). Surface Modification of Bacterial Cellulose Aerogels' Web-like Skeleton for Oil/Water Separation. *ACS Appl. Mater. Interfaces, 7*, 7373–7381.

Saska, S., Raquel, M. S.-C., Lucas, N. T., Leonardo, P. F., Raquel, A. D., Ana Maria, M. G., . . . Younès, M. (2012). Characterization and in vitro evaluation of bacterial cellulose membranes functionalized with osteogenic growth peptide for bone tissue engineering. *J Mater Sci Mater Med., 23*, 2253-2266.

Schacht, K., & Scheibel, T. (2014). Processing of recombinant spider silk proteins into tailor-made materials for biomaterials applications. *Current Opinion in Biotechnology, 29*, 62-69.

Schacht, K., & Scheibel, T. (2014). Processing of recombinant spider silk proteins into tailor-made materials for biomaterials applications. *Current Opinion in Biotechnology, 29*, 62–69.

Schacht, K., & Scheibel, T. (2014). Processing of recombinant spider silk proteins into tailor-made materials for biomaterials applications´. *Current Opinion in Biotechnology, 29*, 62–69.

Scheibel, T. (2004). Spider silks: recombinant synthesis, assembly, spinning, and engineering of synthetic proteins. *Microbial Cell Factories 2004, 3:14, 3*.

Scheibel, T. (2005). Protein fibers as performance proteins: new technologies and applications. *Current Opinion in Biotechnology, 16*, 427–433.

Schulten, K., Dalke, A., & Schulten, K. (1996). VMD Visual Molecular Dynamics. *Journal of Molecular Graphics, 14*, 33-38.

Shao, Z., Young, R. J., & Vollrath, F. (1999). The effect of solvents on spider silk studied by mechanical testing and single-fibre Raman spectroscopy. *International Journal of Biological Macromolecules, 24*, 295-300.

Shea, J.-E., & Brooks III, C. L. (2001). From folding theories to folding proteins: a review and assessment of simulation studies of protein folding and unfolding. *Annual Review of Physical Chemistry, 52*, 499-535.

Sheena Mary, Y., Ushakumari, L., Harikumar, B., Tresa Varghese, H., & Yohannan Panicker, C. (2009). FT-IR, FT-raman and SERS spectra of L-proline. *Journal of the Iranian Chemical Society, 6*, 138-144.

Shinsuke Ifuku, M. T. (2009). Synthesis of Silver Nanoparticles Templated by TEMPO-Mediated Oxidized Bacterial Cellulose Nanofibers. *Biomacromolecules, 10*, 2714-2717.

Simmons, A. H., Michal, C. A., & Jelinski, L. W. (1996). Molecular Orientation and Two-Component Nature of the Crystalline Fraction of Spider Dragline Silk. *SCIENCE, 271*, 84-87.

Simmons, A., Ray, E., & Jelinski, L. W. (1994). Solid-State 13C NMR of Nephila clavipes dragline silk establishes structure and identity of crystalline regions. *Macromolecules, 27*, 5235-5237.

Sintya, E., & Alam, P. (2016). Localised semicrystalline phases of MaSp1 proteins show high sensitivity to overshearing in β-sheet nanocrystals. *International Journal of Biological Macromolecules, 92*, 1006-1011.

Sintya, E., & Alam, P. (2016). Self-assembled semi-crystallinity at parallel β-sheet nanocrystal interfaces in clustered MaSp1 (spider silk) proteins. *Materials Science and Engineering: C, 58*, 366-371.

Siro, I., & Plackett, D. (2010). Microfibrillated cellulose and new nanocomposite materials: a review. *Cellulose, 17*, 459-494.

Songmin Shang, L. Z. (2011). Physical properties of silk fibroin/cellulose blend films regenerated from the hydrophilic ionic liquid. *Carbohydrate Polymers, 86*, 462-468.

Soykeabkaew, N., Sian, C., Gea, S., Nishino, T., & Peijs, T. (2009). All-cellulose nanocomposites by surface selective dissolution of bacterial cellulose. *Cellulose June 2009, Volume 16, Issue 3, pp 435–444, 16*(3), 435-444.

Spaic, M., Small, D. P., Cook, J. R., & Wan, W. (2014). Characterization of anionic and cationic functionalized bacterial cellulose nanofibres for controlled release applications. *Cellulose, 21*, 1529–1540.

Spiess, K., Lammel, A., & Scheibel, T. (2010). Recombinant Spider Silk Proteins for Applications in Biomaterials. *Macromolecular Bioscience, 10*, 998–1007.

Sponner, A., Unger, E., Grosse, F., & Weisshart, K. (2005). Differential polymerization of the two main protein components of dragline silk during fibre spinning. *Nature Materials, 4*, 772-755.

Sponner, A., Vater, W., Monajembashi, S., Unger, E., Grosse, F., & Weisshart, K. (2007). Composition and Hierarchical Organisation of a Spider Silk. *PLoS ONE, 10*, 1-8.

Stein, T. M., Gordon, S. H., & Greene, R. V. (1999). Amino acids as plasticizers II. Use of quantitative structure-property relationships to predict the behavior of monoammoniummonocarboxylate plasticizers in starch–glycerol blends. *Carbohydrate Polymers, 39*, 7–16.

Svensson, A., Nicklasson, E., Harrah, T., Panilaitis, B., Kaplan, D., Brittberg, M., & Gatenholm, P. (2005). Bacterial cellulose as a potential scaffold for tissue engineering of cartilage. *Biomaterials 26 , 26*, 419–431.

Tarakanova, A., & Buehler, M. J. (2012). A Materiomics Approach to Spider Silk: Protein Molecules to Webs. *JOM, 64*.

Teulé, F., Addison, B., Cooper , A., Ayon , J., Henning , R., Benmore , C., . . . Lewis , R.

(2012). Combining flagelliform and dragline spider silk motifs to produce tunable synthetic biopolymer fibers. *Biopolymers, 97*, 418-431.

Teulé, F., Addison, B., Cooper, A. R., Ayon, J., Henning, R. W., Benmore, C. J., . . . Lewis, R. V. (2012). Combining flagelliform and dragline spider silk motifs to produce tunable synthetic biopolymer fibers. *Biopolymers, 97*, 418–431.

Teulé, F., Cooper, A. R., Furin, W. A., Bittencourt, D., Rech, E. L., Brooks, A., & Lewis, R. V. (2009). A protocol for the production of recombinant spider silk-like proteins for artificial fiber spinning. *Nature Protocols, 4*, 341–355.

Torres, F. G., Commeaux, S., & Troncoso, O. P. (2012). Biocompatibility of Bacterial Cellulose Based Biomaterials. *J. Functional Biomaterials, 3*, 864-878.

Touaiti, F., Pahlevan, M., Nilsson, R., Alam, P., Toivakka, M., Ansell, M., & Wilen, C.-E. (2013). Impact of functionalised dispersing agents on the mechanical and viscoelastic properties of pigment coating. *Progress in Organic Coatings, 76*, 101-106.

Ul-Islam, M., Shah, N., Ha, J. H., & Park, J. K. (2011). Effect of chitosan penetration on physico-chemical and mechanical properties of bacterial cellulose. *Korean J. Chem. Eng., 28*, 1736-1743.

Véliz, D. S., Alam, C., Toivola, D. M., Toivakka, M., & Alam, P. (2014). On the non-linear attachment characteristics of blood to bacterial cellulose-kaolin biomaterials. *Colloids and Surfaces B: Biointerfaces, 116*, 176–182.

Vendrely, C., & Scheibel, T. (2007). Biotechnological Production of Spider-Silk Proteins Enables New Applications. *Macromolecular Bioscience, 7*, 401–409.

Vollrath, F., & Knight, D. (2001). Liquid crystalline spinning of spider silk. *Nature, 410*, 541-548.

Volrath, F. (2000). Strength and structure of spiders' silks. *Reviews in Molecular Biotechnology, 74*, 67-83.

Volrath, F., & Porter, D. (2009). Silks as ancient models for modern polymers. *Polymer, 50*, 5623–5632.

Wan, Y., Huang, Y., Yuan, C., Raman, S., Zhu, Y., Jiang, H., . . . Gao, C. (2007). Biomimetic synthesis of hydroxyapatite/bacterial cellulose nanocomposites for biomedical applications. *Materials Science and Engineering C, 27*, 855–864.

Wan, Y., Luo, H., He, F., Liang, H., Huang, Y., & Li, X. (2009). Mechanical, moisture absorption, and biodegradation behaviours of bacterial cellulose fibre-reinforced starch biocomposites. *Composites Science and Technology, 69*, 1212–1217.

Wanna, D. (2012). *Bacterial cellulose-kaolin nanocomposites for application as biomedical wound healing materials.* Åbo Akademi University.

Wanna, D., Alam, C., Toivola, D. M., & Alam, P. (2013). Bacterial cellulose–kaolin nanocomposites for application as biomedical wound healing materials. *Advances in Natural Sciences: Nanoscience and Nanotechnology, 4*.

Wegst, U. G., & Ashby, M. F. (2004). The mechanical efficiency of natural materials. *Philosophical Magazine, 84*, 2167–2181.

Wegst, U. G., Bai, H., Saiz, E., Tomsia, A. P., & Ritchie, R. O. (2015). Bioinspired structural materials. *Nature Materials, 14*, 23-36.

Widhe, M., Bysell, H., Nystedt, S., Nystedt, S., Schenning, I., Malmsten, M., . . . Hedhammar, M. (2010). Recombinant spider silk as matrices for cell culture. *Biomaterials , 31*, 9575-9585.

Widhe, M., Johansson, J., Hedhammar, M., & Rising, A. (2012). Current Progress and Limitations of Spider Silk for Biomedical Applications. *Biopolymers, 97*, 468-478.

Widhe, M., Johansson, U., Hillerdahl, C.-O., & Hedhammar, M. (2013). Recombinant spider silk with cell binding motifs for specific adherence of cells. *Biomaterials, 34*, 8223–8234.

Widhe, M., Shalaly, N., & Hedhammar, M. (2016). A fibronectin mimetic motif improves integrin mediated cell biding to recombinant spider silk matrices. *Biomaterials, 74*, 256-266.

Wohlrab, S., Müller, S., Schmidt, A., Neubauer, S., Kessler, H., Leal-Egaña, A., & Scheibel, T. (2012). Cell adhesion and proliferation on RGD-modified recombinant spider silk proteins. *Biomaterials, 33*, 6650–6659.

Xia, X.-X., Qian, Z.-G., Ki, C., Hwan Park, Y., Kaplan, D., & Yup Lee, S. (2010). Native-sized recombinant spider silk protein produced in metabolically engineered Escherichia coli results in a strong fiber. *PNAS, 107*, 14059–14063.

Yano, S., Maeda, H., Nakajima, M., Hagiwara, T., & Sawaguchi, T. (2008). Preparation and mechanical properties of bacterial cellulose nanocomposites loaded with silica nanoparticles. *Cellulose, 15*(1), 111-120.

Yano, S., Maeda, H., Nakajima, M., Hagiwara, T., & Sawaguchi, T. (2008). Preparation and mechanical properties of bacterial cellulose nanocomposites loaded with silica nanoparticles. *Cellulose, 15*, 111-120.

Yao, J., Chen, S., Chen, Y., Wang, B., Pei, Q., & Wang, H. (2017). Macrofibers with High Mechanical Performance Based on Aligned Bacterial Cellulose Nanofibers. *ACS Appl. Mater. Interfaces*. doi:DOI: 10.1021/acsami.6b14650

Yasutomo Noishiki, Y. N. (2002). Mechanical properties of silk fibroin–microcrystalline cellulose composite films. *J. Appl. Polym. Sci., 86*, 3425–3429.

Yu, Q., Xu, S., Zhang, H., Gu, L., Xu, Y., & Ko, F. (2014). Structure–property relationship of regenerated spider silk protein nano/microfibrous scaffold fabricated by electrospinning. *J Biomed Mater Res Part A, 102A*, 3828–3837.

Zeplin, P. H., Maksimovikj, N. C., Jordan, M. C., Nickel, J., Lang, G., Leimer, A. H., . . . Scheibel, T. (2014). Spider Silk Coatings as a Bioshield to Reduce Periprosthetic Fibrous Capsule Formation. *Adv. Funct. Mater., 24*, 2658–2666.

Zhou, Y., Wu, S., & Conticello, V. P. (2001). Genetically Directed Synthesis and Spectroscopic Analysis of a Protein Polymer Derived from a Flagelliform Silk Sequence. *Biomacromolecules, 2*, 111-125.

Zhu, B., Li, W., Lewis, R. V., Segre, C. U., & Wang, R. (2015). E-Spun Composite Fibers of Collagen and Dragline Silk Protein: Fiber Mechanics, Biocompatibility, and Application in Stem Cell Differentiation. *Biomacromolecules, 16*, 202−213.

7. Publications

Mahdi Pahlevan

Silk-inspired molecular design of bacterial nanocellulose biomaterials

Many material scientists are looking into ways to produce sustainable biomaterials to minimize its footprint on the environment. Biomimetics is utilized for the development of novel synthetic materials that inspired from the formation, function, or structure of biologically produced substances and materials. Spider silks are amongst the toughest materials in nature which exhibit outstanding mechanical performance. The outstanding properties of spider silk have made this material interesting for various industrial and biomedical applications.

ISBN 978-952-12-3972-4